

CERN-EP-2020-136
2021/01/13

CMS-EXO-19-003

Search for dark matter produced in association with a leptonically decaying Z boson in proton-proton collisions at $\sqrt{s} = 13$ TeV

The CMS Collaboration*

Abstract

A search for dark matter particles is performed using events with a Z boson candidate and large missing transverse momentum. The analysis is based on proton-proton collision data at a center-of-mass energy of 13 TeV, collected by the CMS experiment at the LHC in 2016–2018, corresponding to an integrated luminosity of 137 fb^{-1} . The search uses the decay channels $Z \rightarrow ee$ and $Z \rightarrow \mu\mu$. No significant excess of events is observed over the background expected from the standard model. Limits are set on dark matter particle production in the context of simplified models with vector, axial-vector, scalar, and pseudoscalar mediators, as well as on a two-Higgs-doublet model with an additional pseudoscalar mediator. In addition, limits are provided for spin-dependent and spin-independent scattering cross sections and are compared to those from direct-detection experiments. The results are also interpreted in the context of models of invisible Higgs boson decays, unparticles, and large extra dimensions.

*"Published in the European Physical Journal C as
doi:10.1140/epjc/s10052-020-08739-5."*

1 Introduction

The existence of dark matter (DM) is well established from astrophysical observations [1], where the evidence relies entirely on gravitational interactions. According to fits based on the Lambda cold dark matter model of cosmology [2] to observational data, DM comprises 26.4% of the current matter-energy density of the universe, while baryonic matter accounts for only 4.8% [3]. In spite of the abundance of DM, its nature remains unknown. This mystery is the subject of an active experimental program to search for dark matter particles, including direct-detection experiments that search for interactions of ambient DM with ordinary matter, indirect-detection experiments that search for the products of self-annihilation of DM in outer space, and searches at accelerators and colliders that attempt to create DM in the laboratory.

The search presented here considers a “mono-Z” scenario where a Z boson, produced in proton-proton (pp) collisions, recoils against DM or other beyond the standard model (BSM) invisible particles. The Z boson subsequently decays into two charged leptons ($\ell^+\ell^-$, where $\ell = e$ or μ) yielding a dilepton signature, and the accompanying undetected particles contribute to missing transverse momentum. The analysis is based on a data set of pp collisions at a center-of-mass energy of 13 TeV produced at the CERN LHC. The data were recorded with the CMS detector in the years 2016–2018, and correspond to an integrated luminosity of 137 fb^{-1} . The results are interpreted in the context of several models for DM production, as well as for two other scenarios of BSM physics that also predict invisible particles.

These results extend and supersede a previous search by CMS in the mono-Z channel based on a data set collected at $\sqrt{s} = 13 \text{ TeV}$ corresponding to an integrated luminosity of 36 fb^{-1} [4]. The ATLAS experiment has published searches in this channel as well with the latest result based on a data set corresponding to an integrated luminosity of 36 fb^{-1} [5]. Similar searches for DM use other “mono-X” signatures with missing transverse momentum recoiling against a hadronic jet [6, 7], a photon [8], a heavy-flavor (bottom or top) quark [9–11], a W or Z boson decaying to hadrons [5, 7, 12], or a Higgs boson [13–18]. An additional DM interpretation is explored in searches for Higgs boson decays to invisible particles [19, 20].

The paper is organized as follows. The DM and other BSM models explored are introduced along with their relevant parameters in Section 2. Section 3 gives a brief description of the CMS detector. The data and simulated samples are described in Section 4, along with the event reconstruction. The event selection procedures and background estimation methods are described in Sections 5 and 6, respectively. Section 7 details the fitting method implemented for the different models presented, while Section 8 discusses the systematic uncertainties. The results are given in Section 9, and the paper is summarized in Section 10.

2 Signal models

Several models of BSM physics can lead to a signature of a Z boson subsequently decaying into a lepton pair and missing transverse momentum. The goal of this paper is to explore a set of benchmark models for the production of DM that can contribute to this final state. In all DM models we consider, the DM particles are produced in pairs, $\chi\bar{\chi}$, where χ is assumed to be a Dirac fermion.

First, we consider a set of simplified models for DM production [21, 22]. These models describe the phenomenology of DM production at the LHC with a small number of parameters and provide a standard for comparing and combining results from different search channels. Each model contains a massive mediator exchanged in the s-channel, where the mediator (either a

vector, axial-vector, scalar, or pseudoscalar particle) couples directly to quarks and to the DM particle χ . An example tree-level diagram is shown in Fig. 1 (upper left). The free parameters of each model are the mass of the DM particle m_χ , the mass of the mediator m_{med} , the mediator-quark coupling g_q , and the mediator-DM coupling g_χ . Following the suggestions in Ref. [22], for the vector and axial-vector studies, we fix the couplings to values of $g_q = 0.25$ and $g_\chi = 1$ and vary the values of m_χ and m_{med} , and for the scalar and pseudoscalar studies, we fix the couplings $g_q = 1$ and $g_\chi = 1$, set the dark matter particle mass to $m_\chi = 1$ GeV, and vary the values of m_{med} . The comparison with data is carried out separately for each of the four spin-parity choices for the mediator.

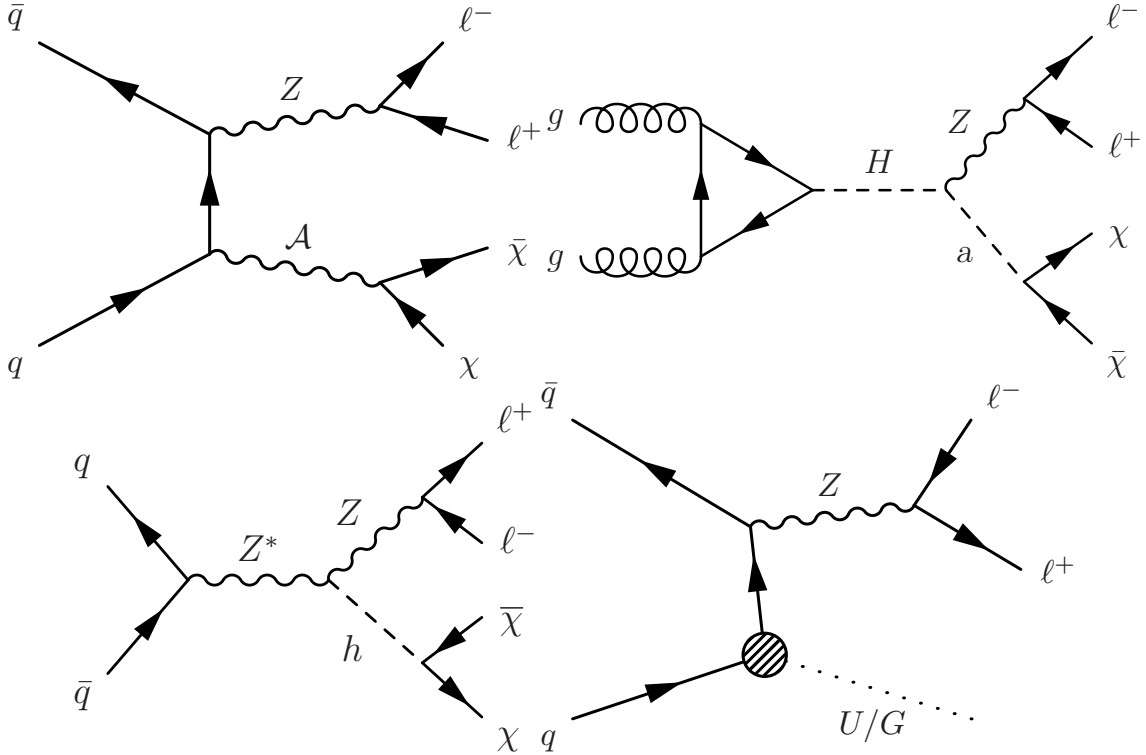


Figure 1: Feynman diagrams illustrative of the BSM processes that produce a final state of a Z boson that decays into a pair of leptons and missing transverse momentum: (upper left) simplified dark matter model for a spin-1 mediator, (upper right) 2HDM+a model, (lower left) invisible Higgs boson decays, and (lower right) graviton (G) production in a model with large extra dimensions or unparticle (U) production. Here A represents the DM mediator, χ represents a DM particle, while (H, h) and a represent the scalar and pseudoscalar Higgs bosons, respectively. Here h is identified with the 125 GeV scalar boson. The dotted line represents either an unparticle or a graviton.

We also explore a two-Higgs-doublet model (2HDM) with an additional pseudoscalar boson, a, that serves as the mediator between DM and ordinary matter. This “2HDM+a” model [23, 24] is a gauge-invariant and renormalizable model that contains a Higgs scalar (h), which we take to be the observed 125 GeV Higgs boson, a heavy neutral Higgs scalar (H), a charged Higgs scalar (H^\pm), and two pseudoscalars (A, a), where the pseudoscalar bosons couple to the DM particles. For the process studied in this paper, the H boson is produced via gluon fusion and decays into a standard model (SM) Z boson and the pseudoscalar a. These subsequently decay into a pair of leptons and a pair of DM particles, respectively, as shown in Fig. 1 (upper right). The sizable couplings of the Z boson to the Higgs bosons makes the mono-Z channel more sensitive to this model than the mono-jet or mono-photon channels. Among the parameters

of this model are the Higgs boson masses, the ratio $\tan\beta$ of the vacuum expectation values of the two Higgs doublets, and the mixing angle θ of the pseudoscalars. We consider only configurations in which $m_H = m_{H^\pm} = m_A$, and fix the values $\tan\beta = 1$ and $\sin\theta = 0.35$, following the recommendations of Ref. [24].

We also examine the case where the h boson acts as a mediator for DM production, as discussed in “Higgs portal” models [25–28]. If $m_\chi < m_h/2$, the Higgs boson could decay invisibly into a pair of DM particles. The mechanism for such decays can be found, for example, in many supersymmetric theoretical models that contain a stable neutral lightest supersymmetric particle, e.g., a neutralino [29], that is sufficiently light. An illustrative Feynman diagram for such a case is shown in Fig. 1 (lower left), while additional gluon-induced diagrams are also considered.

In addition to the DM paradigm, we consider a model where unparticles are responsible for the missing transverse momentum in the final state. The unparticle physics concept [30, 31] is based on scale invariance, which is anticipated in many BSM physics scenarios [32–34]. The effects of the scale-invariant sector (“unparticles”) appear as a non-integral number of invisible massless particles. In this scenario, the SM is extended by introducing a scale-invariant Banks–Zaks field, which has a nontrivial infrared fixed point [35]. This field can interact with the SM particles by exchanging heavy particles with a high mass scale M_U [36]. Below this mass scale, where the coupling is nonrenormalizable, the interaction is suppressed by powers of M_U and can be treated within an effective field theory (EFT). The parameters that characterize the unparticle model are the possible noninteger scaling dimension of the unparticle operator d_U , the coupling of the unparticles to SM fields λ , and the cutoff scale of the EFT Λ_U . In order to remain in the EFT regime, the cutoff scale is set to $\Lambda_U = 15$ TeV and to maintain unitarity, only $d_U > 1$ is considered. Figure 1 (lower right) shows the tree-level diagram considered in this paper for the production of unparticles associated with a Z boson.

The final SM extension considered in this paper is the Arkani-Hamed–Dimopoulos–Dvali (ADD) model of large extra dimensions [37, 38], which is motivated by the disparity between the electroweak (EW) unification scale ($M_{EW} \sim 100$ GeV) and the Planck scale ($M_{Pl} \sim 10^{19}$ GeV). This model predicts graviton (G) production via the process $q\bar{q} \rightarrow Z + G$, as shown in Fig. 1 (lower right). The graviton escapes detection, leading to a mono-Z signature. In the ADD model, the apparent Planck scale in four spacetime dimensions is given by $M_{Pl}^2 \approx M_D^{n+2} R^n$, where M_D is the fundamental Planck scale in the full $(n+4)$ -dimensional spacetime and R is the compactification length scale of the extra dimensions. Assuming M_D is of the same order as M_{EW} , the observed large value of M_{Pl} suggests values of R much larger than the Planck length. These values are on the order of nm for $n = 3$, decreasing with larger values of n . The consequence of the large compactification scale is that the mass spectrum of the Kaluza–Klein graviton states becomes nearly continuous [37, 38], resulting in a broadened spectrum for the transverse momentum (p_T) of the Z boson.

3 The CMS detector

The central feature of the CMS apparatus is a superconducting solenoid of 6 m internal diameter, providing a magnetic field of 3.8 T. Within the solenoid volume are a silicon pixel and strip tracker, a lead tungstate crystal electromagnetic calorimeter (ECAL), and a brass and scintillator hadron calorimeter (HCAL), each composed of a barrel and two endcap sections. Forward calorimeters extend the pseudorapidity (η) coverage provided by the barrel and endcap detectors. Muons are detected in gas-ionization chambers embedded in the steel flux-return yoke outside the solenoid.

Events of interest are selected using a two-tiered trigger system [39]. The first level (L1), composed of custom hardware processors, uses information from the calorimeters and muon detectors to select events at a rate of around 100 kHz within a time interval of less than $4 \mu\text{s}$. The second level, known as the high-level trigger (HLT), consists of a farm of processors running a version of the full event reconstruction software optimized for fast processing, and reduces the event rate to around 1 kHz before data storage.

A more detailed description of the CMS detector, together with a definition of the coordinate system used and the relevant kinematic variables, can be found in Ref. [40].

4 Data samples and event reconstruction

This search uses pp collision events collected with the CMS detector during 2016, 2017, and 2018 corresponding to a total integrated luminosity of 137 fb^{-1} . The data sets from the three different years are analyzed independently with appropriate calibrations and corrections to take into account the different LHC running conditions and CMS detector performance.

Several SM processes can contribute to the mono-Z signature. The most important backgrounds come from diboson processes: $WZ \rightarrow \ell\nu\ell\ell$ where one lepton escapes detection, $ZZ \rightarrow \ell\nu\nu$, and $WW \rightarrow \ell\nu\nu$. There can also be contributions where energetic leptons are produced by decays of top quarks in $t\bar{t}$ or tW events. Smaller contributions may come from triple vector boson processes (WWZ , WZZ , and ZZZ), $t\bar{t}W \rightarrow WWb\bar{b}W$, $t\bar{t}Z \rightarrow WWb\bar{b}Z$, and $t\bar{t}\gamma \rightarrow WWb\bar{b}\gamma$, referred to collectively as VVV due to the similar decay products. Drell-Yan (DY) production of lepton pairs, $Z/\gamma^* \rightarrow \ell\ell$, has no intrinsic source of missing transverse momentum but can still mimic a mono-Z signature when the momentum of the recoiling system is poorly measured. A minor source of background is from events with a vector boson and a misreconstructed photon, referred to as $V\gamma$.

Monte Carlo simulated events are used to model the expected signal and background yields. Three sets of simulated events for each process are used in order to match the different data taking conditions. The samples for DM production are generated using the DMSIMP package [41, 42] interfaced with MADGRAPH5_aMC@NLO 2.4.2 [43–46]. The pseudoscalar and scalar model samples are generated at leading order (LO) in quantum chromodynamics (QCD), while the vector and axial-vector model samples are generated at next-to-leading-order (NLO) in QCD. The POWHEGv2 [47–51] generator is used to simulate the Zh signal process of the invisible Higgs boson at NLO in QCD, as well as the $t\bar{t}$, tW , and diboson processes. The BSM Higgs boson production cross sections, as a function of the Higgs boson mass for the Zh process are taken from Refs. [52]. Samples for the 2HDM+a model are generated at NLO with MADGRAPH5_aMC@NLO 2.6.0. Events for both the ADD and unparticle models are generated at LO using an EFT implementation in PYTHIA 8.205 in 2016 and 8.230 in 2017 and 2018 [53, 54]. In order to ensure the validity of the effective theory used in the ADD model, a truncation method, described in Ref. [55], is applied. Perturbative calculations are only valid in cases where the square of the center-of-mass energy (\hat{s}) of the incoming partons is smaller than the fundamental scale of the theory (M_{D}^2). As such, this truncation method suppresses the cross section for events with $\hat{s} > M_{\text{D}}^2$ by a factor of M_{D}^4/\hat{s}^2 . The effect of this truncation is largest for small values of M_{D} , but also increases with the number of dimensions n as more energy is lost in extra dimensions. The MADGRAPH5_aMC@NLO 2.2.2 (2.4.2) generator in 2016 (2017 and 2018) is used for the simulation of the VVV, $V\gamma$, and DY samples, at NLO accuracy in QCD.

The set of parton distribution functions (PDFs) used for simulating the 2016 sample is NNPDF 3.0 NLO [56] and for the 2017 and 2018 samples it is NNPDF 3.1 NNLO. For all processes, the

parton showering and hadronization are simulated using PYTHIA 8.226 in 2016 and 8.230 in 2017 and 2018. The modeling of the underlying event is generated using the CUETP8M1 [57] (CP5 [58]) for simulated samples corresponding to the 2016 (2017 and 2018) data sets. The only exceptions to this are the 2016 top quark sample, which uses CUETP8M2 [57] and the simplified DM (2HDM+a) samples, which uses CP3 [58] (CP5) tunes for all years. All events are processed through a simulation of the CMS detector based on GEANT4 [59] and are reconstructed with the same algorithms as used for data. Simultaneous pp collisions in the same or nearby bunch crossings, referred to as pileup, are also simulated. The distribution of the number of such interactions in the simulation is chosen to match the data, with periodic adjustments to take account of changes in LHC operating conditions [60]. The average number of pileup interactions was 23 for the 2016 data and 32 for the 2017 and 2018 data.

Information from all subdetectors is combined and used by the CMS particle-flow (PF) algorithm [61] for particle reconstruction and identification. The PF algorithm aims to reconstruct and identify each individual particle in an event, with an optimized combination of information from the various elements of the CMS detector. The energies of photons are obtained from the ECAL measurement. The energies of electrons are determined from a combination of the electron momentum at the primary interaction vertex as determined by the tracker, the energy from the corresponding ECAL cluster, and the energy sum from all bremsstrahlung photons spatially compatible with originating from the electron track. The momentum of muons is obtained from the curvature of the corresponding track in the tracker detector in combination with information from the muon stations. The energies of charged hadrons are determined from a combination of their momentum measured in the tracker and the matching ECAL and HCAL energy deposits, corrected for the response function of the calorimeters to hadronic showers. Finally, the energies of neutral hadrons are obtained from the corresponding corrected ECAL and HCAL energies.

The candidate vertex with the largest value of summed physics-object p_T^2 is taken to be the primary pp interaction vertex. The physics objects are the jets, clustered using the jet finding algorithm [62, 63] with the tracks assigned to candidate vertices as inputs, and the associated missing transverse momentum, taken as the negative vector sum of the p_T of those jets.

Both electron and muon candidates must pass certain identification criteria to be further selected in the analysis. They must satisfy requirements on the transverse momentum and pseudorapidity: $p_T > 10$ GeV and $|\eta| < 2.5$ (2.4) for electrons (muons). At the final level, a medium working point [64, 65] is chosen for the identification criteria, including requirements on the impact parameter of the candidates with respect to the primary vertex and their isolation with respect to other particles in the event. The efficiencies for these selections are about 85 and 90% for each electron and muon, respectively.

In the signal models considered in this paper, the amount of hadronic activity tends to be small, so events with multiple clustered jets are vetoed. For each event, hadronic jets are clustered from reconstructed particle candidates using the infrared and collinear safe anti- k_T algorithm [62, 63] with a distance parameter of 0.4. Jet momentum is determined as the vectorial sum of all particle momenta in the jet, and is found from simulation to be, on average, within 5 to 10% of the true momentum over the entire spectrum and detector acceptance. Pileup interactions can contribute additional tracks and calorimetric energy depositions to the jet momentum. To mitigate this effect, charged particles identified to be originating from pileup vertices are discarded and an offset is applied to correct for remaining contributions [66]. Jet energy corrections are derived from simulation to bring the measured response of jets to the average of simulated jets clustered from the generated final-state particles. In situ measurements

of the momentum balance in dijet, photon+jet, Z+jet, and multijet events are used to determine corrections for residual differences between jet energy scale in data and simulation [66]. The jet energy resolution amounts typically to 15% at 10 GeV, 8% at 100 GeV, and 4% at 1 TeV. Additional selection criteria are applied to each jet to remove jets potentially dominated by anomalous contributions from some subdetector components or reconstruction failures [67]. Jets with $p_T > 30$ GeV and $|\eta| < 4.7$ are considered for the analysis.

To identify jets that originated from b quarks, we use the medium working point of the DeepCSV algorithm [68]. This selection was chosen to remove events from top quark decays originating specifically from $t\bar{t}$ production, without causing a significant loss of signal. For this working point, the efficiency to select b quark jets is about 70% and the probability for mistagging jets originating from the hadronization of gluons or u/d/s quarks is about 1% in simulated $t\bar{t}$ events.

To identify hadronically decaying τ leptons (τ_h), we use the hadron-plus-strips algorithm [69]. This algorithm constructs candidates seeded by PF jets that are consistent with either a single or triple charged pion decay of the τ lepton. In the single charged pion decay mode, the presence of neutral pions is detected by reconstructing their photonic decays. Mistagged jets originating from non- τ decays are rejected by a discriminator that takes into account the pileup contribution to the neutral component of the τ_h decay [69]. The efficiency to select real hadronically decaying τ leptons is about 75% and the probability for mistagging jets is about 1%.

The missing transverse momentum vector \vec{p}_T^{miss} is computed as the negative vector sum of the transverse momenta of all the PF candidates in an event, and its magnitude is denoted as p_T^{miss} [70]. The \vec{p}_T^{miss} is modified to account for corrections to the energy scale of the reconstructed jets in the event. Events with anomalously high p_T^{miss} can originate from a variety of reconstruction failures, detector malfunctions, or noncollision backgrounds. Such events are rejected by event filters that are designed to identify more than 85–90% of the spurious high- p_T^{miss} events with a misidentification rate of less than 0.1% [70].

5 Event selection

Events with electrons (muons) are collected using dielectron (dimuon) triggers, with thresholds of $p_T > 23$ (17) GeV and $p_T > 12$ (8) GeV for the electron (muon) with the highest and second-highest measured p_T , respectively. Single-electron and single-muon triggers with p_T thresholds of 25 (27) and 20 (24) GeV for 2016 (2017–2018) are used to recover residual inefficiencies, ensuring a trigger efficiency above 99% for events passing the offline selection.

In the signal region (SR), events are required to have two ($N_\ell = 2$) well-identified, isolated electrons or muons with the same flavor and opposite charge (e^+e^- or $\mu^+\mu^-$). At least one electron or muon of the pair must have $p_T > 25$ GeV, while the second must have $p_T > 20$ GeV. In order to reduce nonresonant background, the dilepton invariant mass is required to be within 15 GeV of the world-average Z boson mass m_Z [71]. Additionally, we require the p_T of the dilepton system $p_T^{\ell\ell}$ to be larger than 60 GeV to reject the bulk of the DY background. Since little hadronic activity is expected for the signal, we reject events having more than one jet with $p_T > 30$ GeV within $|\eta| < 4.7$. The top quark background is further suppressed by rejecting events containing any b-tagged jet with $p_T > 30$ GeV reconstructed within the tracker acceptance of $|\eta| < 2.4$. To reduce the WZ background in which both bosons decay leptonically, we remove events containing additional electrons or muons with loose identification and with $p_T > 10$ GeV. Events containing a loosely identified τ_h candidate with $p_T > 18$ GeV and $|\eta| < 2.3$ are also rejected. Decays that are consistent with production of muons or electrons are rejected by an overlap

veto.

In addition to the above criteria, there are several selections designed to further reduce the SM background. The main discriminating variables are: the missing transverse momentum, p_T^{miss} ; the azimuthal angle formed between the dilepton p_T and the \vec{p}_T^{miss} , $\Delta\phi(\vec{p}_T^{\ell\ell}, \vec{p}_T^{\text{miss}})$; and the balance ratio, $|p_T^{\text{miss}} - p_T^{\ell\ell}|/p_T^{\ell\ell}$. The latter two variables are especially powerful in rejecting DY and top quark processes. Selection criteria are optimized to obtain the best signal sensitivity for the range of DM processes considered. The final selection requirements are: $p_T^{\text{miss}} > 100$ GeV, $\Delta\phi(\vec{p}_T^{\ell\ell}, \vec{p}_T^{\text{miss}}) > 2.6$ radians, and $|p_T^{\text{miss}} - p_T^{\ell\ell}|/p_T^{\ell\ell} < 0.4$.

For the 2HDM+a model, the selection differs slightly. We make a less stringent requirement on the missing transverse momentum, $p_T^{\text{miss}} > 80$ GeV, and require the transverse mass, $m_T = \sqrt{2p_T^{\ell\ell}p_T^{\text{miss}}[1 - \cos \Delta\phi(\vec{p}_T^{\ell\ell}, \vec{p}_T^{\text{miss}})]}$ to be greater than 200 GeV. The kinematic properties of the 2HDM+a production yield a peak in the m_T spectrum near the neutral Higgs scalar (H) mass that is advantageous for background discrimination.

In order to avoid biases in the p_T^{miss} calculation due to jet mismeasurement, events with one jet are required to have the azimuthal angle between this jet and the missing transverse momentum, $\Delta\phi(\vec{p}_T^j, \vec{p}_T^{\text{miss}})$, larger than 0.5 radians. To reduce the contribution from backgrounds such as WW and tt, we apply a requirement on the distance between the two leptons in the (η, ϕ) plane, $\Delta R_{\ell\ell} < 1.8$, where $\Delta R_{\ell\ell} = \sqrt{(\Delta\phi_{\ell\ell})^2 + (\Delta\eta_{\ell\ell})^2}$.

A summary of the selection criteria for the SR is given in Table 1.

Table 1: Summary of the kinematic selections for the signal region.

Quantity	Requirement	Target backgrounds
N_ℓ	=2 with additional lepton veto	WZ, VVV
p_T^ℓ	>25/20 GeV for leading/subleading	Multijet
Dilepton mass	$ m_{\ell\ell} - m_Z < 15$ GeV	WW, top quark
Number of jets	≤ 1 jet with $p_T^j > 30$ GeV	DY, top quark, VVV
$p_T^{\ell\ell}$	>60 GeV	DY
b tagging veto	0 b-tagged jet with $p_T > 30$ GeV	Top quark, VVV
τ lepton veto	0 τ_h cand. with $p_T^\tau > 18$ GeV	WZ
$\Delta\phi(\vec{p}_T^j, \vec{p}_T^{\text{miss}})$	>0.5 radians	DY, WZ
$\Delta\phi(\vec{p}_T^{\ell\ell}, \vec{p}_T^{\text{miss}})$	>2.6 radians	DY
$ p_T^{\text{miss}} - p_T^{\ell\ell} /p_T^{\ell\ell}$	<0.4	DY
$\Delta R_{\ell\ell}$	<1.8	WW, top quark
p_T^{miss} (all but 2HDM+a)	>100 GeV	DY, WW, top quark
p_T^{miss} (2HDM+a only)	>80 GeV	DY, WW, top quark
m_T (2HDM+a only)	>200 GeV	DY, WW, ZZ, top quark

6 Background estimation

We estimate the background contributions using combined information from simulation and control regions (CRs) in data. A simultaneous maximum likelihood fit to the p_T^{miss} or m_T distributions in the SR and CRs constrains the background normalizations and their uncertainties. Specific CRs target different categories of background processes, as described below.

6.1 The three-lepton control region

The $WZ \rightarrow \ell'v\ell\ell$ decay mode can contribute to the SR when the third lepton ($\ell' = e$ or μ) escapes detection, and this same process can be monitored in an orthogonal CR, where the third lepton is identified and then removed. The construction of the three-lepton (3ℓ) CR is based on events with three well-reconstructed charged leptons. A Z boson candidate is selected in the same manner as for the SR, while an additional electron or muon with identical quality and isolation is required. In cases where there are multiple Z boson candidates, the candidate with invariant mass closest to the Z boson mass is selected. To enhance the purity of the WZ selection, p_T^{miss} of at least 30 GeV is required and the invariant mass of three leptons is required to be larger than 100 GeV. The backgrounds in this CR are similar to those in the SR, with a sizable nonprompt background from DY events where a jet is misidentified as a lepton [72]. An additional minor source of background is from events with a vector boson and a misreconstructed photon ($V\gamma$). All background estimates for this CR are taken from simulation.

To simulate the consequences of not detecting the third lepton, the “emulated p_T^{miss} ” is estimated from the vectorial sum of \vec{p}_T^{miss} and the transverse momentum (\vec{p}_T) of the additional lepton. The emulated p_T^{miss} is then used in place of the reconstructed p_T^{miss} and the same selection is applied as for the SR. Since there is negligible contamination from $WZ \rightarrow \tau\nu\ell\ell$ and top quark backgrounds in this CR, no veto is applied on additional τ_h or b jet candidates. The resulting emulated p_T^{miss} spectrum is shown in Fig. 2 (left). For the 2HDM+a case, the “emulated m_T ” is used instead of “emulated p_T^{miss} ” with the same selections.

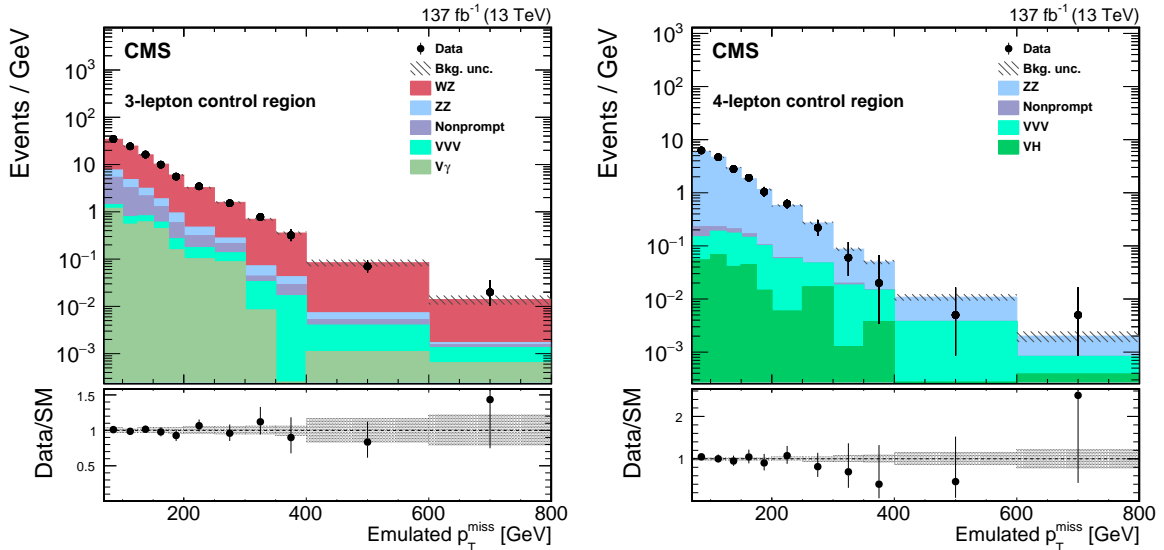


Figure 2: Emulated p_T^{miss} distribution in data and simulation for the 3ℓ (left) and 4ℓ (right) CRs. Uncertainty bands correspond to the postfit combined statistical and systematic components, where the fitting method is described in Section 7.

6.2 The four-lepton control region

The ZZ process contributes to the SR through the $ZZ \rightarrow \ell\ell\nu\nu$ decay mode, and the same production process can be monitored via the decay mode $ZZ \rightarrow 4\ell$. The 4ℓ CR is based on events with two pairs of charged leptons. Each pair comprises two leptons of opposite charge and the same flavor and corresponds to a Z candidate. Two of the four leptons must fulfill the same requirements on the leptons as in the SR, while, in order to increase the yield, the other two leptons need only pass relaxed lepton quality requirements. The highest p_T Z boson candidate is required to have an invariant mass within 35 GeV of the Z boson mass m_Z [71].

Additionally, we require the transverse momentum of this Z boson candidate to be larger than 60 GeV. Additional backgrounds to the ZZ final state are events from triboson processes, events with a vector boson and a higgs boson (Vh) and from nonprompt events. These backgrounds are almost negligible. All background estimates for this CR are taken from simulation.

For these four-lepton events, the emulated p_T^{miss} is calculated as the vectorial sum of the \vec{p}_T^{miss} and the \vec{p}_T of the Z boson candidate with the larger absolute mass difference to m_Z . The choice of which Z boson to use as a proxy for an invisibly decaying boson negligibly alters the emulated p_T^{miss} spectrum. The same selection as the SR is then applied using the emulated p_T^{miss} in place of the reconstructed p_T^{miss} , with the exception of the τ_h and b jet candidate vetoes. The resulting emulated p_T^{miss} spectrum is shown in Fig. 2 (right). Similarly to the 3ℓ CR, the “emulated m_T ” is used instead of “emulated p_T^{miss} ” for the 2HDM+a case and the distribution is well described by the SM background estimations.

6.3 The electron-muon control region

We estimate the contribution of the flavor-symmetric backgrounds from an $e\mu$ CR based on events with two leptons of different flavor and opposite charge ($e^\pm\mu^\mp$) that pass all other analysis selections. This CR is largely populated by nonresonant backgrounds (NRB) consisting mainly of leptonic W boson decays in $t\bar{t}$, tW , and WW events, where the dilepton mass happens to fall inside the Z boson mass window. Small contributions from single top quark events produced via s - and t -channel processes, and $Z \rightarrow \tau\tau$ events in which τ leptons decay into light leptons and neutrinos, are also considered in the NRB estimation.

6.4 The DY control region

The DY background is dominant in the region of low p_T^{miss} . This process does not produce undetectable particles. Therefore, any nonzero p_T^{miss} arises from mismeasurement or limitations in the detector acceptance. The estimation of this background uses simulated DY events, for which the normalization is taken from data in a sideband CR of $80 < p_T^{\text{miss}} < 100$ GeV where the signal contamination is negligible, with all other selections applied. For the 2HDM+a analysis, a similar approach is taken with relaxed p_T^{miss} selection of $50 < p_T^{\text{miss}} < 100$ GeV and an additional selection of $m_T < 200$ GeV applied. The sideband CR is included in the maximum likelihood fit and a 100% uncertainty is assigned to the extrapolation from this CR to the SR. This uncertainty has little effect on the results because of the smallness of the overall contribution from the DY process in the SR.

7 Fitting method

After applying the selection, we perform a binned maximum likelihood fit to discriminate between the potential signal and the remaining background processes. The data sets for each data-taking year are kept separate in the fit. This yields a better expected significance than combining them into a single set because the signal-to-background ratios are different for the three years due to the different data-taking conditions. The electron and muon channels have comparable signal-to-background ratios, and are combined in the fit, while the contributions, corrections and systematic uncertainties are calculated individually.

The p_T^{miss} distribution of events passing the selection is used as the discriminating variable in the fit for all of the signal hypotheses except for the 2HDM+a model. For this model, the m_T distribution is used since a Jacobian peak around the pseudoscalar Higgs boson mass is expected. Events in the SR are split into 0-jet and 1-jet categories to take into account the different

signal-to-background ratios. In addition, for the CRs defined in Section 6, events with 0-jet and 1-jet are included as a single category in the fit. The $e\mu$ and DY CRs are each included as a single bin corresponding to the total yield. The p_T^{miss} or m_T spectra in the 3ℓ and 4ℓ CRs are included in the fit with the same binning as in the SR, where these spectra are based upon the emulated p_T^{miss} . To allow for further freedom in the ZZ and WZ background estimation, the p_T^{miss} and emulated p_T^{miss} distributions are split into three regions with independent normalization parameters: low (<200 GeV), medium (200–400 GeV), and high (>400 GeV), with uncertainties of 10, 20, and 30%, respectively. These values are based on the magnitudes of the theoretical uncertainties as described in Section 8. For fits to the 2HDM+a model, three similar m_T regions are chosen with the same uncertainties: low (<400 GeV), medium (400–800 GeV), and high (>800 GeV). To make the best use of the statistical power in the CRs and to take advantage of the similarities of the production processes, we take the normalization factors to be correlated for the ZZ and the WZ backgrounds in each p_T^{miss} region.

For each individual bin, a Poisson likelihood term describes the fluctuation of the data around the expected central value, which is given by the sum of the contributions from signal and background processes. Systematic uncertainties are represented by nuisance parameters θ with log-normal probability density functions used for normalization uncertainties and Gaussian functions used for shape-based uncertainties, with the functions centered on their nominal values $\hat{\theta}$. The uncertainties affect the overall normalizations of the signal and background templates, as well as the shapes of the predictions across the distributions of observables. Correlations among systematic uncertainties in different categories are taken into account as discussed in Section 8. The total likelihood is defined as the product of the likelihoods of the individual bins and the probability density functions for the nuisance parameters:

$$\mathcal{L} = \mathcal{L}_{\text{SR}} \mathcal{L}_{3\ell} \mathcal{L}_{4\ell} \mathcal{L}_{e\mu} \mathcal{L}_{\text{DY}} f_{\text{NP}}(\theta | \hat{\theta}) \quad (1)$$

The factors of the likelihood can be written more explicitly as

$$\mathcal{L}_{\text{SR}} = \prod_{i,j} \mathcal{P}\left(N_{\text{obs},i,j}^{\text{SR}} \mid \mu_{\text{DY}} N_{\text{DY},i,j}^{\text{SR}}(\theta) + \mu_{\text{NRB}} N_{\text{NRB},i,j}^{\text{SR}}(\theta) + N_{\text{other},i,j}^{\text{SR}}(\theta) + \mu_{\text{VV},r(i)} (N_{\text{ZZ},i,j}^{2\ell}(\theta) + N_{\text{WZ},i,j}^{\text{SR}}(\theta)) + \mu N_{\text{Sig},i,j}^{\text{SR}}(\theta)\right), \quad (2)$$

$$\mathcal{L}_{3\ell} = \prod_i \mathcal{P}\left(N_{\text{obs},i}^{3\ell} \mid N_{\text{other},i}^{3\ell}(\theta) + \mu_{\text{VV},r(i)} N_{\text{WZ},i}^{3\ell}(\theta)\right), \quad (3)$$

$$\mathcal{L}_{4\ell} = \prod_i \mathcal{P}\left(N_{\text{obs},i}^{4\ell} \mid N_{\text{other},i}^{4\ell}(\theta) + \mu_{\text{VV},r(i)} N_{\text{ZZ},i}^{4\ell}(\theta)\right), \quad (4)$$

$$\mathcal{L}_{e\mu} = \mathcal{P}\left(N_{\text{obs}}^{e\mu} \mid \mu_{\text{NRB}} N_{\text{NRB}}^{e\mu}(\theta) + N_{\text{other}}^{e\mu}(\theta)\right), \quad (5)$$

$$\mathcal{L}_{\text{DY}} = \mathcal{P}\left(N_{\text{obs}}^{\text{DY}} \mid \mu_{\text{DY}} N_{\text{DY}}^{\text{DY}}(\theta) + \mu_{\text{NRB}} N_{\text{NRB}}^{\text{DY}}(\theta) + N_{\text{other}}^{\text{DY}}(\theta) + N_{\text{ZZ}}^{\text{DY}}(\theta) + N_{\text{WZ}}^{\text{DY}}(\theta) + \mu N_{\text{Sig}}^{\text{DY}}(\theta)\right). \quad (6)$$

The purpose of the fit is to determine the confidence interval for the signal strengths μ . Here $\mathcal{P}(N | \lambda)$ is the Poisson probability to observe N events for an expected value of λ , and $f_{\text{NP}}(\theta | \hat{\theta})$ describes the nuisance parameters with log-normal probability density functions used for normalization uncertainties and Gaussian functions used for shape-based uncertainties. The index i indicates the bin of the p_T^{miss} or m_T distribution, $r(i)$ corresponds to the region (low, medium, high) of bin i , and the index j indicates the 0-jet or 1-jet selection. The diboson process normalization in the region $r(i)$ is $\mu_{\text{VV},r(i)}$, while μ_{DY} is the DY background

normalization and μ_{NRB} is the normalization for the nonresonant background. The yield prediction from simulation for process x in region y is noted as N_x^y . The smaller backgrounds in each region are merged together and are indicated collectively as "other". The method above for constructing likelihood functions follows that of Ref. [73], where a more detailed mathematical description may be found.

8 Systematic uncertainties

In the following, we describe all of the uncertainties that are taken into account in the maximum likelihood fit. We consider the systematic effects on both the overall normalization and on the shape of the distribution of p_T^{miss} or m_T for all applicable uncertainties. We evaluate the impacts by performing the full analysis with the value of the relevant parameters shifted up and down by one standard deviation. The final varied distributions of p_T^{miss} or m_T are used for signal extraction and as input to the fit. For each source of uncertainty, variations in the distributions are thus treated as fully correlated, while independent sources of uncertainty are treated as uncorrelated. Except where noted otherwise, the systematic uncertainties for the three different years of data taking are treated as correlated.

The assigned uncertainties in the integrated luminosity are 2.5, 2.3, and 2.5% for the 2016, 2017, and 2018 data samples [74–76], respectively, and are treated as uncorrelated across the different years.

We apply scale factors to all simulated samples to correct for discrepancies in the lepton reconstruction and identification efficiencies between data and simulation. These factors are measured using DY events in the Z boson peak region [65, 77, 78] that are recorded with unbiased triggers. The factors depend on the lepton p_T and η and are within a few percent of unity for electrons and muons. The uncertainty in the determination of the trigger efficiency leads to an uncertainty smaller than 1% in the expected signal yield.

For the kinematic regions used in this analysis, the lepton momentum scale uncertainty for both electrons and muons is well represented by a constant value of 0.5%. The uncertainty in the calibration of the jet energy scale (JES) and resolution directly affects the p_T^{miss} computation and all the selection requirements related to jets. The estimate of the JES uncertainty is performed by varying the JES. The variation corresponds to a re-scaling of the jet four-momentum as $p \rightarrow p(1 \pm \delta p_T^{\text{JES}} / p_T)$, where δp_T^{JES} is the absolute uncertainty in the JES, which is parameterized as function of the p_T and η of the jet. In order to account for the systematic uncertainty from the jet resolution smearing procedure, the resolution scale factors are varied within their uncertainties. Since the uncertainties in the JES are derived independently for the three data sets, they are treated as uncorrelated across the three data sets.

The signal processes are expected to produce very few events containing b jets, and we reject events with any jets that satisfy the b tagging algorithm working point used. In order to account for the b tagging efficiencies observed in data, an event-by-event reweighting using b tagging scale factors and efficiencies is applied to simulated events. The uncertainty is obtained by varying the event-by-event weight by ± 1 standard deviation. Since the uncertainties in the b tagging are derived independently for the three data sets, they are treated as uncorrelated across the three data sets. The variation of the final yields induced by this procedure is less than 1%.

Simulated samples are reweighted to reproduce the pileup conditions observed in data. We evaluate the uncertainty related to pileup by recalculating these weights for variations in the

total inelastic cross section by 5% around the nominal value [79]. The resulting shift in weights is propagated through the analysis and the corresponding p_T^{miss} and m_T spectra are used as input to the maximum likelihood fit. The variation of the final yields induced by this procedure is less than 1%.

Shape-based uncertainties for the ZZ and WZ backgrounds, referred to jointly as VV, and signal processes are derived from variations of the renormalization and factorization scales, the strong coupling constant α_S , and PDFs [80–82]. The scales are varied up and down by a factor of two. Variations of the PDF set and α_S are used to estimate the corresponding uncertainties in the yields of the signal and background processes following Ref. [56]. The missing higher-order EW terms in the event generation for the VV processes yield another source of theoretical uncertainty [83, 84]. The following additional higher-order corrections are applied: a constant (approximately 10%) correction for the WZ cross section from NLO to NNLO in QCD calculations [85]; a constant (approximately 3%) correction for the WZ cross section from LO to NLO in EW calculations, according to Ref. [86]; a $\Delta\phi(Z, Z)$ -dependent correction to the ZZ production cross section from NLO to next-to-next-to-leading order (NNLO) in QCD calculations [87]; a p_T -dependent correction to the ZZ cross section from LO to NLO in EW calculations, following Refs. [83, 84, 86], which is the dominant correction in the signal region. We use the product of the above NLO EW \times NLO QCD corrections [88] as an estimate of the missing NLO EW \times NLO QCD contribution, which is not used as a correction, but rather assigned as an uncertainty. The resulting variations in the p_T^{miss} and m_T distribution are used as a shape uncertainty in the likelihood fit.

The shapes of the p_T^{miss} and m_T distributions are needed for each of the background processes. For the DY and nonresonant processes, we take the shape directly from simulation. The distributions for the ZZ and WZ processes are obtained by taking the shapes from the simulation and normalizing them to the yield seen in the data in the CR. The gluon-induced and the quark-induced ZZ processes have different acceptances and their uncertainties are treated separately, while the normalization factors are taken to be correlated. In all cases, the limited number of simulated events in any given bin gives rise to a systematic uncertainty. This uncertainty is treated as fully uncorrelated across the bins and processes.

A summary of the impact on the signal strength of the systematic uncertainties is shown in Table 2. The Zh(invisible) model is used as an example to illustrate the size of the uncertainties, both for the presence ($\mathcal{B}(h \rightarrow \text{invisible}) = 1$) and absence ($\mathcal{B}(h \rightarrow \text{invisible}) = 0$) of a signal. These two paradigms are used to generate Asimov data sets that are then fit to give the uncertainty estimates shown in Table 2. The systematic uncertainties are dominated by the theoretical uncertainty in the ZZ and WZ background contributions.

9 Results

The number of observed and expected events in the SR after the final selection is given in Table 3, where the values of the expected yields and their uncertainties are obtained from the maximum likelihood fit. The observed numbers of events are compatible with the background predictions. The expected yields and the product of acceptance and efficiency for several signal models used in the analysis are shown in Table 4. The post-fit p_T^{miss} distributions for events in the signal region in the 0-jet and 1-jet categories are shown in Fig. 3. The final m_T distributions used for the 2HDM+a model are shown in Fig. 4.

For each of the models considered, simulated signal samples are generated for relevant sets of model parameters. The observed p_T^{miss} and m_T spectra are used to set limits on theories of

Table 2: Summary of the uncertainties in the branching fraction arising from the systematic uncertainties considered in the $Zh(\text{invisible})$ model assuming $\mathcal{B}(h \rightarrow \text{invisible}) = 1$ (signal) and $\mathcal{B}(h \rightarrow \text{invisible}) = 0$ (no signal). Here, lepton measurement refers to the combined trigger, lepton reconstruction and identification efficiencies, and the lepton momentum and electron energy scale systematic uncertainty. Theory uncertainties include variations of the renormalization and factorization scales, α_s , and PDFs as well as the higher-order EWK corrections.

Source of uncertainty	Impact assuming signal	Impact assuming no signal
Integrated luminosity	0.013	0.002
Lepton measurement	0.032	0.050
Jet energy scale and resolution	0.042	0.024
Pileup	0.012	0.009
b tagging efficiency	0.004	0.002
Theory	0.088	0.085
Simulation sample size	0.024	0.023
Total systematic uncertainty	0.11	0.11
Statistical uncertainty	0.089	0.073
Total uncertainty	0.14	0.13

Table 3: Observed number of events and post-fit background estimates in the two jet multiplicity categories of the SR. The reported uncertainty represents the sum in quadrature of the statistical and systematic components.

Process	0-jet category	1-jet category
Drell-Yan	502 ± 94	1179 ± 64
WZ	1479 ± 53	389 ± 16
ZZ	670 ± 27	282 ± 13
Nonresonant background	384 ± 31	263 ± 22
Other background	6.3 ± 0.7	6.8 ± 0.8
Total background	3040 ± 110	2120 ± 76
Data	3053	2142

Table 4: Expected yields and the product of acceptance and efficiency for several models probed in the analysis. The quoted values correspond to the $Z \rightarrow \ell\ell$ decays. The reported uncertainty represents the sum in quadrature of the statistical and systematic components.

Model	Yields	Product of acceptance and efficiency (%)
Zh(125)	864 ± 64	10.6 ± 0.8
ADD $M_{\text{D}} = 3 \text{ TeV}, n = 4$	35.1 ± 2.4	18.6 ± 1.3
Unparticle $S_{\text{U}} = 0, d_{\text{U}} = 1.50$	221 ± 16	8.2 ± 0.6
2HDM+a $m_{\text{H}} = 1000 \text{ GeV}, m_{\text{a}} = 400 \text{ GeV}$	14.1 ± 4.0	12.7 ± 2.7
DM Vector $m_{\text{med}} = 1000 \text{ GeV}, m_{\chi} = 1 \text{ GeV}$	64.8 ± 6.1	17.6 ± 1.7

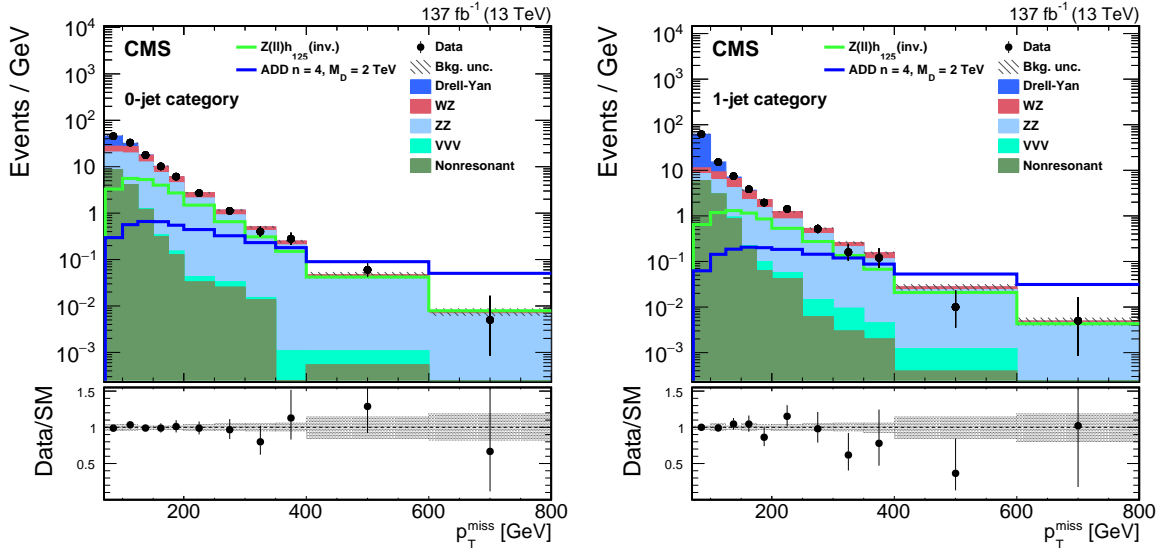


Figure 3: The p_T^{miss} distributions for events in the signal region in the 0-jet (left) and 1-jet (right) categories. The rightmost bin also includes events with $p_T^{\text{miss}} > 800$ GeV. The uncertainty band includes both statistical and systematic components. The Zh(invisible) signal normalization assumes SM production rates and the branching fraction $\mathcal{B}(h \rightarrow \text{invisible}) = 1$. For the ADD model, the signal normalization assumes the expected values for $n = 4$ and $M_D = 2$ TeV.

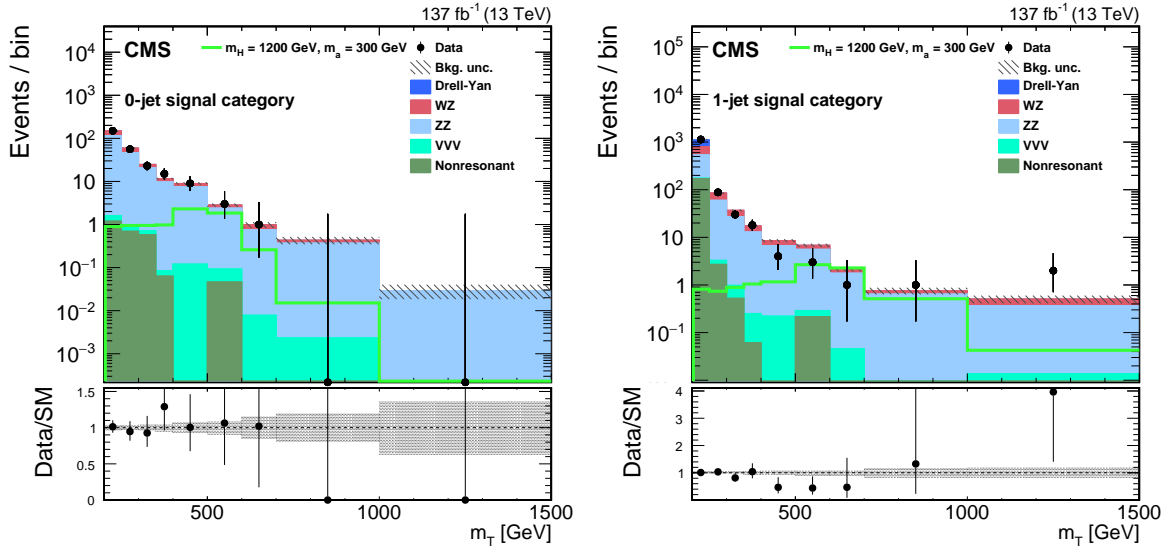


Figure 4: The m_T distributions for events in the signal region in the 0-jet (left) and 1-jet (right) categories. The rightmost bin includes all events with $m_T > 1000$ GeV. The uncertainty band includes both statistical and systematic components. The signal normalization assumes the expected values for $m_H = 1200$ GeV, $m_a = 300$ GeV within the 2HDM+a framework where $m_H = m_{H^\pm} = m_A$, $\tan \beta = 1$ and $\sin \theta = 0.35$.

new physics using the modified frequentist construction CL_s [73, 89, 90] used in the asymptotic approximation [91].

9.1 Simplified dark matter model interpretation

In the framework of the simplified models of DM, the signal production is sensitive to the mass, spin, and parity of the mediator as well as the coupling strengths of the mediator to quarks and to DM. The p_T^{miss} distribution is used as an input to the fit. Limits for the vector and axial-vector mediators are shown as a function of the mediator mass m_{med} and DM particle mass m_χ as shown in Figure 5. Cosmological constraints on the DM abundance [92] are added to Fig. 5 where the shaded area represents the region where additional physics would be needed to describe the DM abundance. For vector mediators, we observe a limit around $m_{\text{med}} > 870$ GeV for most values of m_χ less than $m_{\text{med}}/2$. For axial-vector mediators the highest limit reached in the allowed region is about $m_{\text{med}} > 800$ GeV. In both cases, the previous limits from this channel are extended by about 150 GeV, but the limits are still less restrictive than those from published mono-jet results [7] because weakly coupled Z bosons are radiated from the initial state quarks much less frequently than gluons. Figure 6 shows the 90% CL limits on the DM-nucleon cross sections calculated following the suggestions in Ref. [22]. Limits are shown as a function of the DM particle mass for both the spin-independent and spin-dependent cases and compared to selected results from direct-detection experiments.

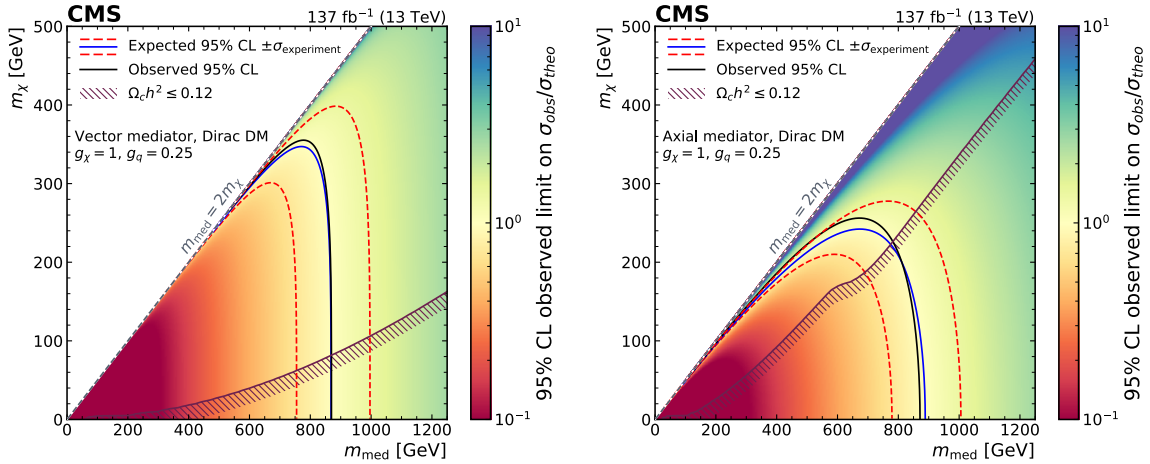


Figure 5: The 95% CL exclusion limits for the vector (left) and the axial-vector (right) simplified models. The limits are shown as a function of the mediator and DM particle masses. The coupling to quarks is fixed to $g_q = 0.25$ and the coupling to DM is set to $g_\chi = 1$.

In addition to vector and axial-vector mediators, scalar and pseudoscalar mediators are also tested. For these models, we fix both couplings to quarks and to DM particles: $g_q = 1$ and $g_\chi = 1$ as suggested in Ref. [22]. Since the choice of DM particle mass is shown to have negligible effects on the kinematic distributions of the detected particles, we set it to the constant value of $m_\chi = 1$ GeV. Figure 7 gives the 95% CL exclusion limits on the production cross section

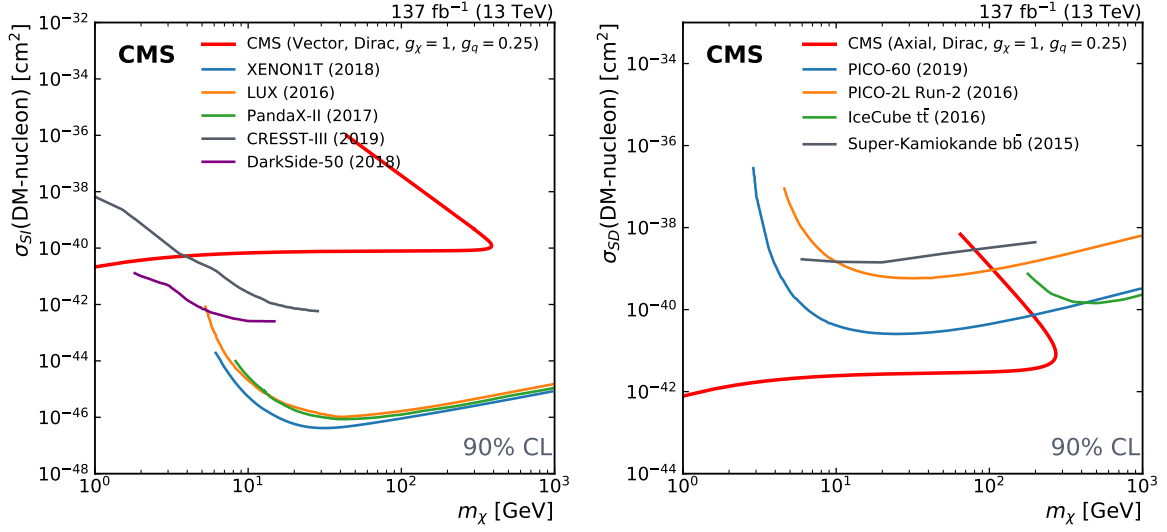


Figure 6: The 90% CL DM-nucleon upper limits on the cross section for simplified DM in the spin-independent (left) and spin-dependent (right) cases. The coupling to quarks is set to $g_q = 0.25$ and the coupling to DM is set to $g_\chi = 1$. Limits from the XENON1T [93], LUX [94], PandaX-II [95], CRESST-III [96], and DarkSide-50 [97] experiments are shown for the spin-independent case with vector couplings. Limits from the PICO-60 [98], PICO-2L [99], IceCube [100], and Super-Kamiokande [101] experiments are shown for the spin-dependent case with axial-vector couplings.

over the predicted cross section as a function of the mediator mass m_{med} . The expected limits are about 25% better than the previous results in this channel [4], but are not yet sensitive enough to exclude any value of m_{med} . The best limits obtained on the cross section are about 1.5 times larger than the predicted values for low values of m_{med} .

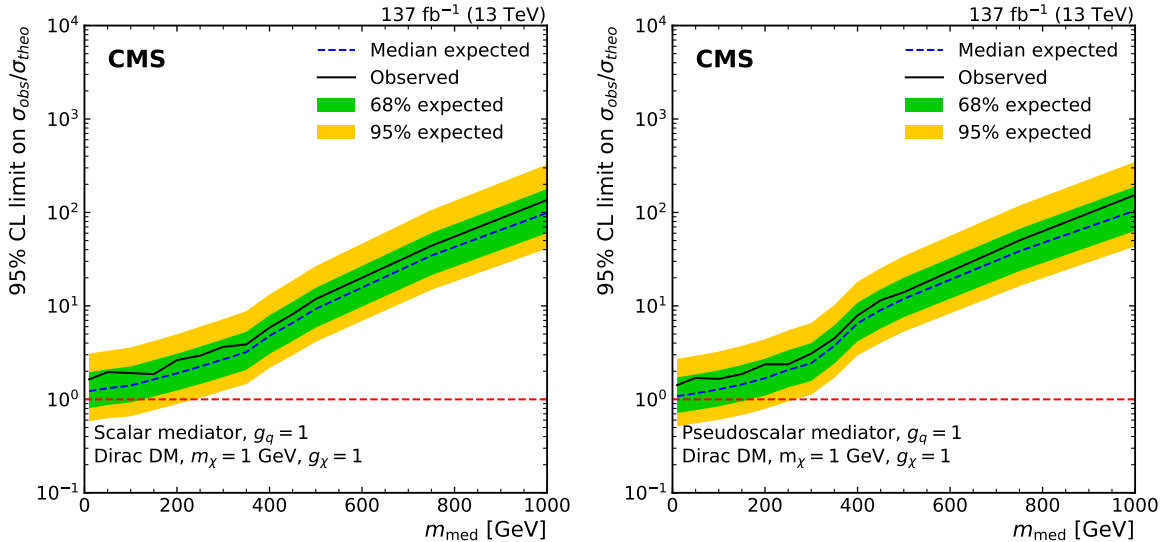


Figure 7: The 95% CL upper limits on the cross section for simplified DM models with scalar (left) and pseudoscalar (right) mediators. The coupling to quarks is set to $g_q = 1$, the coupling to DM is set to $g_\chi = 1$ and the DM mass is $m_\chi = 1$ GeV.

9.2 Two-Higgs-doublet model interpretation

For the 2HDM+a model, the signal production is sensitive to the heavy Higgs boson and the pseudoscalar a masses. As discussed in Section 7, the m_T distribution is used in the fit rather than p_T^{miss} . The limits on both the heavy Higgs boson and the additional pseudoscalar mediator a are shown in Fig. 8. The mixing angles are set to $\tan \beta = 1$ and $\sin \theta = 0.35$ with a DM particle mass of $m_\chi = 10$ GeV. The mediator mass with the most sensitivity is $m_H = 1000$ GeV, where the observed (expected) limit on m_a is 440 (340) GeV. For small values of m_a , the limit on m_H is about 1200 GeV. These can be compared with the observed (expected) limits from ATLAS of $m_a > 340$ (340) GeV and $m_H > 1050$ (1000) GeV based on a $\sqrt{s} = 13$ TeV data set corresponding to an integrated luminosity of 36 fb^{-1} [102].

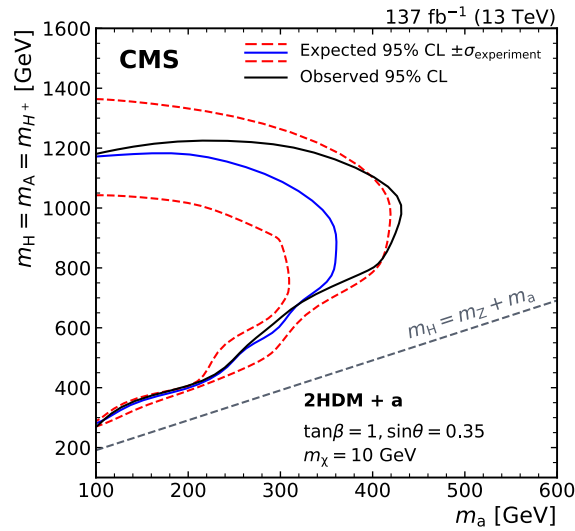


Figure 8: The 95% CL upper limits on the 2HDM+a model with the mixing angles set to $\tan \beta = 1$ and $\sin \theta = 0.35$ and with a DM particle mass of $m_\chi = 10$ GeV. The limits are shown as a function of the heavy Higgs boson and the pseudoscalar masses.

9.3 Invisible Higgs boson interpretation

For the search for invisible decays of the Higgs boson, we use the p_T^{miss} distribution as input to the fit. We obtain upper limits on the product of the Higgs boson production cross section and branching fraction to invisible particles $\sigma_{Z_h} \mathcal{B}(h \rightarrow \text{invisible})$. This can be interpreted as an upper limit on $\mathcal{B}(h \rightarrow \text{invisible})$ by assuming the production rate [52, 103, 104] for an SM Higgs boson at $m_h = 125$ GeV. The observed (expected) 95% CL upper limit at $m_h = 125$ GeV on $\mathcal{B}(h \rightarrow \text{invisible})$ is 29% ($25_{-7}^{+9}\%$) as shown in Fig. 9. The observed (expected) limit from the previous CMS result in this channel was $\mathcal{B}(h \rightarrow \text{invisible}) < 45(44)\%$. The combinations of all earlier results yields an observed (expected) limit of 19 (15)% from CMS [19] and 26% ($17_{-5}^{+5}\%$) from ATLAS [20].

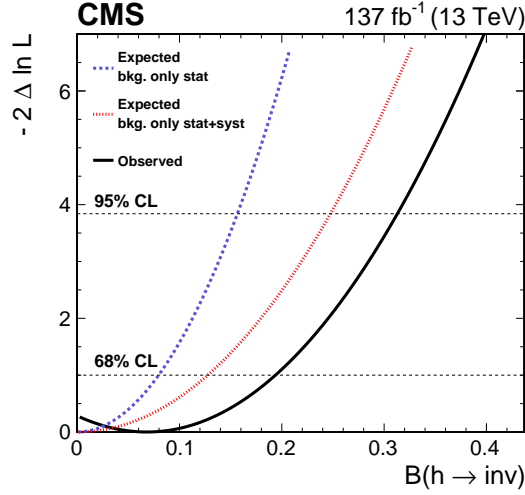


Figure 9: The value of the negative log-likelihood, $-2\Delta\ln\mathcal{L}$, as a function of the branching fraction of the Higgs boson decaying to invisible particles.

9.4 Unparticle interpretation

In the unparticle scenario, the same analysis of the p_T^{miss} spectrum is performed. At 95% CL, upper limits are set on the cross section with $\Lambda_U = 15$ TeV. The limits are shown in Fig. 10 as a function of the scaling dimension d_U . The observed (expected) limits are 0.5 (0.7) pb, 0.24 (0.26) pb, and 0.09 (0.07) pb for $d_U = 1$, $d_U = 1.5$, and $d_U = 2$ respectively, compared to 1.0 (1.0) pb, 0.4 (0.4) pb, and 0.15 (0.15) pb for the earlier result [4]. These limits depend on the choice of λ and Λ_U , as the cross section scales with the Wilson coefficient λ/Λ_U [30]. We fix the coupling between the SM and the unparticle fields to $\lambda = 1$.

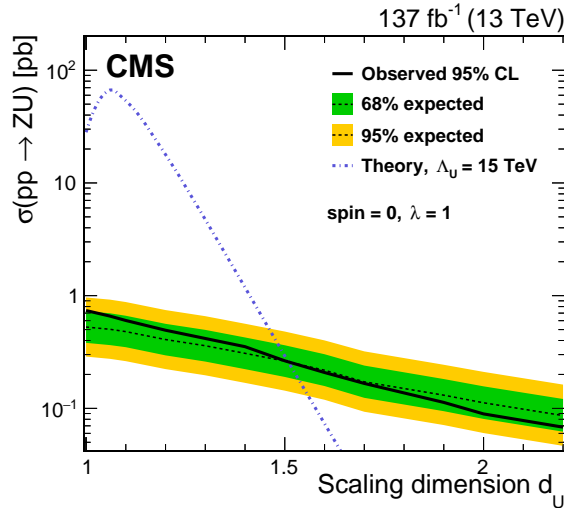


Figure 10: The 95% CL upper limits on unparticle+Z production cross section, as a function of the scaling dimension d_U . These limits apply to fixed values of the effective cutoff scale $\Lambda_U = 15$ TeV and coupling $\lambda = 1$.

9.5 The ADD Interpretation

In the framework of the ADD model of extra dimensions, we use the fits to the p_T^{miss} distribution to calculate limits on the number of extra dimensions n and the fundamental Planck scale M_D . The cross section limit calculated as a function of M_D for the case where $n = 4$ is shown in Fig. 11. The limits on M_D as a function of n are obtained, as shown in Fig. 12. The observed (expected) 95% CL exclusion upper limit on the mass M_D is 2.9–3.0 (2.7–2.8) TeV compared to earlier results of 2.3–2.5 (2.3–2.5) TeV [4].

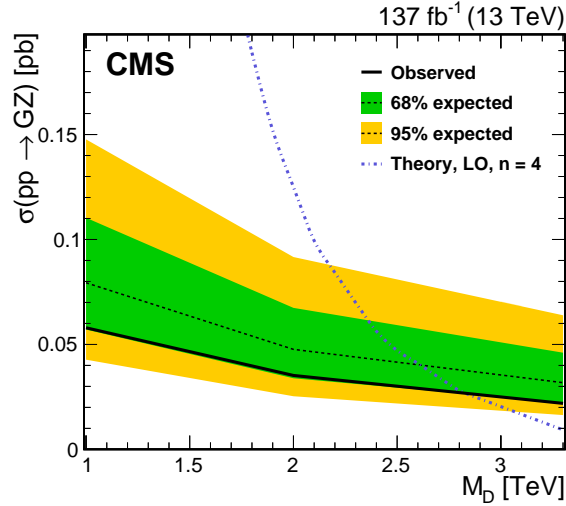


Figure 11: The 95% CL cross section limit in the ADD scenario as a function of M_D for $n = 4$.

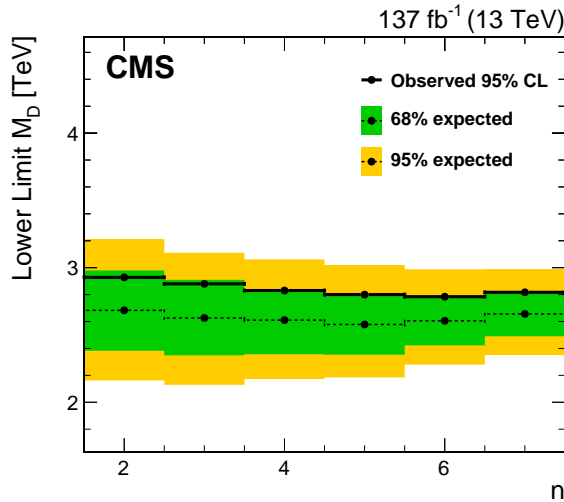


Figure 12: The 95% CL expected and observed exclusion limits on M_D as a function of the number of extra dimensions n .

9.6 Summary of limits

Table 5 gives a summary of the limits expected and observed for a selection of relevant parameters in all of the models considered.

Table 5: Observed and expected 95% CL limits on parameters for the simplified DM models, invisible decays of the Higgs boson, two-Higgs-doublet model, large extra dimensions in the ADD scenario, and unparticle model. For the scalar and pseudoscalar mediators, the limits are dependent on the mediator mass, so the lowest values for the ratio of observed to theoretical cross sections are presented. For the vector and axial-vector mediators, the limits are dependent on the DM particle mass, so the limits are shown for $m_\chi < 300$ GeV for the vector mediator and $m_\chi = 240$ GeV for the axial-vector mediator.

Model	Parameter	Observed	Expected
DM - vector $g_\chi = 1$ $g_q = 0.25$	m_{med}	870 GeV	870 GeV
DM - axial-vector $g_\chi = 1$ $g_q = 0.25$	m_{med}	800 GeV	800 GeV
DM - scalar $g_\chi = 1$ $g_q = 1$ $m_\chi = 1$ GeV	$\sigma_{\text{obs}}/\sigma_{\text{theo}}$	1.8	1.5
DM - pseudoscalar $g_\chi = 1$ $g_q = 1$ $m_\chi = 1$ GeV	$\sigma_{\text{obs}}/\sigma_{\text{theo}}$	1.8	1.4
2HDM+a $\tan \beta = 1$ $m_\chi = 1$ GeV $\sin \theta = 0.35$ $m_H = m_A = 1$ TeV	m_a	330 GeV	440 GeV
2HDM+a $\tan \beta = 1$ $m_\chi = 1$ GeV $\sin \theta = 0.35$ $m_a = 100$ GeV	m_H	1200 GeV	1200 GeV
Invisible Higgs boson	$\mathcal{B}(h \rightarrow \text{invisible})$	0.29	0.25
ADD $n = 2-7$	M_D	2.8–2.9 TeV	2.6–2.7 TeV
Unparticles Scaling dimension $d_U=1.5$	σ	0.26 pb	0.24 pb

10 Summary

Events with a Z boson recoiling against missing transverse momentum in proton-proton collisions at the LHC are used to search for physics beyond the standard model. The results are interpreted in the context of several different models of the coupling mechanism between dark matter and ordinary matter: simplified models of dark matter with vector, axial-vector, scalar, and pseudoscalar mediators; invisible decays of a 125 GeV scalar Higgs boson; and a two-Higgs-doublet model with an extra pseudoscalar. Outside the context of dark matter, models that invoke large extra dimensions or propose the production of unparticles could contribute to the same signature and are also considered. The observed limits on the production cross sections are used to constrain parameters of each of these models. The search utilizes a data set collected by the CMS experiment in 2016–2018, corresponding to an integrated luminosity of 137 fb^{-1} at $\sqrt{s} = 13 \text{ TeV}$. No evidence of physics beyond the standard model is observed. Comparing to the previous results in this channel based on a partial data sample collected at $\sqrt{s} = 13 \text{ TeV}$ in 2016, corresponding to an integrated luminosity of approximately 36 fb^{-1} for CMS [4] and for ATLAS [5], the exclusion limits for simplified dark matter mediators, gravitons and unparticles are significantly extended. For the case of a 125 GeV scalar boson, an upper limit of 29% is set for the branching fraction to fully invisible decays at 95% confidence level. Results for the two-Higgs-doublet model with an additional pseudoscalar are presented in this final state and probe masses of the pseudoscalar mediator up to 440 GeV and of the heavy Higgs boson up to 1200 GeV when the other model parameters are set to specific benchmark values.

Acknowledgments

We congratulate our colleagues in the CERN accelerator departments for the excellent performance of the LHC and thank the technical and administrative staffs at CERN and at other CMS institutes for their contributions to the success of the CMS effort. In addition, we gratefully acknowledge the computing centers and personnel of the Worldwide LHC Computing Grid for delivering so effectively the computing infrastructure essential to our analyses. Finally, we acknowledge the enduring support for the construction and operation of the LHC and the CMS detector provided by the following funding agencies: BMBWF and FWF (Austria); FNRS and FWO (Belgium); CNPq, CAPES, FAPERJ, FAPERGS, and FAPESP (Brazil); MES (Bulgaria); CERN; CAS, MoST, and NSFC (China); COLCIENCIAS (Colombia); MSES and CSF (Croatia); RIF (Cyprus); SENESCYT (Ecuador); MoER, ERC IUT, PUT and ERDF (Estonia); Academy of Finland, MEC, and HIP (Finland); CEA and CNRS/IN2P3 (France); BMBF, DFG, and HGF (Germany); GSRT (Greece); NKFI (Hungary); DAE and DST (India); IPM (Iran); SFI (Ireland); INFN (Italy); MSIP and NRF (Republic of Korea); MES (Latvia); LAS (Lithuania); MOE and UM (Malaysia); BUAP, CINVESTAV, CONACYT, LNS, SEP, and UASLP-FAI (Mexico); MOS (Montenegro); MBIE (New Zealand); PAEC (Pakistan); MSHE and NSC (Poland); FCT (Portugal); JINR (Dubna); MON, RosAtom, RAS, RFBR, and NRC KI (Russia); MESTD (Serbia); SEIDI, CPAN, PCTI, and FEDER (Spain); MOSTR (Sri Lanka); Swiss Funding Agencies (Switzerland); MST (Taipei); ThEPCenter, IPST, STAR, and NSTDA (Thailand); TUBITAK and TAEK (Turkey); NASU (Ukraine); STFC (United Kingdom); DOE and NSF (USA).

Individuals have received support from the Marie-Curie program and the European Research Council and Horizon 2020 Grant, contract Nos. 675440, 752730, and 765710 (European Union); the Leventis Foundation; the A.P. Sloan Foundation; the Alexander von Humboldt Foundation; the Belgian Federal Science Policy Office; the Fonds pour la Formation à la Recherche dans l'Industrie et dans l'Agriculture (FRIA-Belgium); the Agentschap voor Innovatie door

Wetenschap en Technologie (IWT-Belgium); the F.R.S.-FNRS and FWO (Belgium) under the “Excellence of Science – EOS” – be.h project n. 30820817; the Beijing Municipal Science & Technology Commission, No. Z191100007219010; the Ministry of Education, Youth and Sports (MEYS) of the Czech Republic; the Deutsche Forschungsgemeinschaft (DFG) under Germany’s Excellence Strategy – EXC 2121 “Quantum Universe” – 390833306; the Lendület (“Momentum”) Program and the János Bolyai Research Scholarship of the Hungarian Academy of Sciences, the New National Excellence Program ÚNKP, the NKFIA research grants 123842, 123959, 124845, 124850, 125105, 128713, 128786, and 129058 (Hungary); the Council of Science and Industrial Research, India; the HOMING PLUS program of the Foundation for Polish Science, cofinanced from European Union, Regional Development Fund, the Mobility Plus program of the Ministry of Science and Higher Education, the National Science Center (Poland), contracts Harmonia 2014/14/M/ST2/00428, Opus 2014/13/B/ST2/02543, 2014/15/B/ST2/03998, and 2015/19/B/ST2/02861, Sonata-bis 2012/07/E/ST2/01406; the National Priorities Research Program by Qatar National Research Fund; the Ministry of Science and Higher Education, project no. 02.a03.21.0005 (Russia); the Programa Estatal de Fomento de la Investigación Científica y Técnica de Excelencia María de Maeztu, grant MDM-2015-0509 and the Programa Severo Ochoa del Principado de Asturias; the Thalís and Aristeia programs cofinanced by EU-ESF and the Greek NSRF; the Rachadapisek Sompot Fund for Postdoctoral Fellowship, Chulalongkorn University and the Chulalongkorn Academic into Its 2nd Century Project Advancement Project (Thailand); the Kavli Foundation; the Nvidia Corporation; the SuperMicro Corporation; the Welch Foundation, contract C-1845; and the Weston Havens Foundation (USA).

References

- [1] G. Bertone and D. Hooper, “History of dark matter”, *Rev. Mod. Phys.* **90** (2018) 045002, doi:10.1103/RevModPhys.90.045002, arXiv:1605.04909.
- [2] S. F. Daniel et al., “Testing general relativity with current cosmological data”, *Phys. Rev. D* **81** (2010) 123508, doi:10.1103/PhysRevD.81.123508, arXiv:1002.1962.
- [3] Planck Collaboration, “Planck 2018 results. I. overview and the cosmological legacy of Planck”, (2018). arXiv:1807.06205.
- [4] CMS Collaboration, “Search for new physics in events with a leptonically decaying Z boson and a large transverse momentum imbalance in proton-proton collisions at $\sqrt{s} = 13$ TeV”, *Eur. Phys. J. C* **78** (2018) 291, doi:10.1140/epjc/s10052-018-5740-1, arXiv:1711.00431.
- [5] ATLAS Collaboration, “Search for an invisibly decaying Higgs boson or dark matter candidates produced in association with a Z boson in pp collisions at $\sqrt{s} = 13$ TeV with the ATLAS detector”, *Phys. Lett. B* **776** (2018) 318, doi:10.1016/j.physletb.2017.11.049, arXiv:1708.09624.
- [6] ATLAS Collaboration, “Search for dark matter and other new phenomena in events with an energetic jet and large missing transverse momentum using the ATLAS detector”, *JHEP* **01** (2018) 126, doi:10.1007/JHEP01(2018)126, arXiv:1711.03301.
- [7] CMS Collaboration, “Search for new physics in final states with an energetic jet or a hadronically decaying W or Z boson and transverse momentum imbalance at $\sqrt{s} = 13$ TeV”, *Phys. Rev. D* **97** (2018) 092005, doi:10.1103/PhysRevD.97.092005, arXiv:1712.02345.

- [8] ATLAS Collaboration, “Search for dark matter at $\sqrt{s} = 13$ TeV in final states containing an energetic photon and large missing transverse momentum with the ATLAS detector”, *Eur. Phys. J. C* **77** (2017) 393, doi:10.1140/epjc/s10052-017-4965-8, arXiv:1704.03848.
- [9] ATLAS Collaboration, “Search for dark matter produced in association with bottom or top quarks in $\sqrt{s} = 13$ TeV pp collisions with the ATLAS detector”, *Eur. Phys. J. C* **78** (2018) 18, doi:10.1140/epjc/s10052-017-5486-1, arXiv:1710.11412.
- [10] ATLAS Collaboration, “Search for a scalar partner of the top quark in the all-hadronic $t\bar{t}$ plus missing transverse momentum final state at $\sqrt{s} = 13$ TeV with the ATLAS detector”, *Eur. Phys. J. C* **80** (2020), no. 8, 737, doi:10.1140/epjc/s10052-020-8102-8, arXiv:2004.14060.
- [11] CMS Collaboration, “Search for dark matter in events with energetic, hadronically decaying top quarks and missing transverse momentum at $\sqrt{s} = 13$ TeV”, *JHEP* **06** (2018) 027, doi:10.1007/JHEP06(2018)027, arXiv:1801.08427.
- [12] ATLAS Collaboration, “Search for dark matter in events with a hadronically decaying vector boson and missing transverse momentum in pp collisions at $\sqrt{s} = 13$ TeV with the ATLAS detector”, *JHEP* **10** (2018) 180, doi:10.1007/JHEP10(2018)180, arXiv:1807.11471.
- [13] ATLAS Collaboration, “Search for dark matter in association with a Higgs boson decaying to two photons at $\sqrt{s} = 13$ TeV with the atlas detector”, *Phys. Rev. D* **96** (2017) 112004, doi:10.1103/PhysRevD.96.112004, arXiv:1706.03948.
- [14] ATLAS Collaboration, “Search for dark matter produced in association with a Higgs boson decaying to $b\bar{b}$ using 36 fb⁻¹ of pp collisions at $\sqrt{s} = 13$ TeV with the ATLAS detector”, *Phys. Rev. Lett.* **119** (2017) 181804, doi:10.1103/PhysRevLett.119.181804, arXiv:1707.01302.
- [15] CMS Collaboration, “Search for heavy resonances decaying into a vector boson and a Higgs boson in final states with charged leptons, neutrinos and b quarks at $\sqrt{s} = 13$ TeV”, *JHEP* **11** (2018) 172, doi:10.1007/JHEP11(2018)172, arXiv:1807.02826.
- [16] CMS Collaboration, “Search for dark matter produced in association with a Higgs boson decaying to a pair of bottom quarks in proton-proton collisions at $\sqrt{s} = 13$ TeV”, *Eur. Phys. J. C* **79** (2019) 280, doi:10.1140/epjc/s10052-019-6730-7, arXiv:1811.06562.
- [17] CMS Collaboration, “Search for dark matter produced in association with a Higgs boson decaying to $\gamma\gamma$ or $\tau^+\tau^-$ at $\sqrt{s} = 13$ TeV”, *JHEP* **09** (2018) 046, doi:10.1007/JHEP09(2018)046, arXiv:1806.04771.
- [18] CMS Collaboration, “Search for dark matter particles produced in association with a Higgs boson in proton-proton collisions at $\sqrt{s} = 13$ TeV”, *JHEP* **03** (2020) 025, doi:10.1007/JHEP03(2020)025, arXiv:1908.01713.
- [19] CMS Collaboration, “Search for invisible decays of a Higgs boson produced through vector boson fusion in proton-proton collisions at $\sqrt{s} = 13$ TeV”, *Phys. Lett. B* **793** (2019) 520, doi:10.1016/j.physletb.2019.04.025, arXiv:1809.05937.

-
- [20] ATLAS Collaboration, “Combination of searches for invisible Higgs boson decays with the ATLAS experiment”, *Phys. Rev. Lett.* **122** (2019) 231801, doi:10.1103/PhysRevLett.122.231801, arXiv:1904.05105.
- [21] LHC Dark Matter Forum (Abercrombie, D. et al.), “Dark matter benchmark models for early LHC Run-2 searches: report of the ATLAS/CMS dark matter forum”, *Phys. Dark Univ.* **27** (2020) 100371, doi:10.1016/j.dark.2019.100371, arXiv:1507.00966.
- [22] LHC Dark Matter Working Group, “Recommendations on presenting LHC searches for missing transverse energy signals using simplified s-channel models of dark matter”, *Phys. Dark Univ.* **27** (2020) 100365, doi:10.1016/j.dark.2019.100365, arXiv:1603.04156.
- [23] M. Bauer, U. Haisch, and F. Kahlhoefer, “Simplified dark matter models with two Higgs doublets: I. pseudoscalar mediators”, *JHEP* **05** (2017) 138, doi:10.1007/JHEP05(2017)138, arXiv:1701.07427.
- [24] LHC Dark Matter Working Group, “LHC Dark Matter Working Group: next-generation spin-0 dark matter models”, *Phys. Dark Univ.* **27** (2020) 100351, doi:10.1016/j.dark.2019.100351, arXiv:1810.09420.
- [25] S. Baek, P. Ko, W.-I. Park, and E. Senaha, “Higgs portal vector dark matter : revisited”, *JHEP* **05** (2013) 036, doi:10.1007/JHEP05(2013)036, arXiv:1212.2131.
- [26] A. Djouadi, O. Lebedev, Y. Mambrini, and J. Quevillon, “Implications of LHC searches for Higgs–portal dark matter”, *Phys. Lett. B* **709** (2012) 65, doi:10.1016/j.physletb.2012.01.062, arXiv:1112.3299.
- [27] A. Djouadi, A. Falkowski, Y. Mambrini, and J. Quevillon, “Direct detection of Higgs-portal dark matter at the LHC”, *Eur. Phys. J. C* **73** (2013) 2455, doi:10.1140/epjc/s10052-013-2455-1, arXiv:1205.3169.
- [28] G. Arcadi, A. Djouadi, and M. Raidal, “Dark matter through the Higgs portal”, *Phys. Rept.* **842** (2020) 1, doi:10.1016/j.physrep.2019.11.003, arXiv:1903.03616.
- [29] G. Belanger et al., “The MSSM invisible Higgs in the light of dark matter and g-2”, *Phys. Lett. B* **519** (2001) 93, doi:10.1016/S0370-2693(01)00976-5, arXiv:hep-ph/0106275.
- [30] H. Georgi, “Unparticle physics”, *Phys. Rev. Lett.* **98** (2007) 221601, doi:10.1103/PhysRevLett.98.221601, arXiv:hep-ph/0703260.
- [31] H. Georgi, “Another odd thing about unparticle physics”, *Phys. Lett. B* **650** (2007) 275, doi:10.1016/j.physletb.2007.05.037, arXiv:0704.2457.
- [32] Z. Kang, “Upgrading sterile neutrino dark matter to FIMP using scale invariance”, *Eur. Phys. J. C* **75** (2015) 471, doi:10.1140/epjc/s10052-015-3702-4, arXiv:1411.2773.
- [33] M. Rinaldi, G. Cognola, L. Vanzo, and S. Zerbini, “Inflation in scale-invariant theories of gravity”, *Phys. Rev. D* **91** (2015) 123527, doi:10.1103/PhysRevD.91.123527, arXiv:1410.0631.
- [34] H. Cheng, “The possible existence of Weyl’s vector meson”, *Phys. Rev. Lett.* **61** (1988) 2182, doi:10.1103/PhysRevLett.61.2182.

- [35] T. Banks and A. Zaks, "On the phase structure of vector-like gauge theories with massless fermions", *Nucl. Phys. B* **196** (1982) 189, doi:10.1016/0550-3213(82)90035-9.
- [36] K. Cheung, W.-Y. Keung, and T.-C. Yuan, "Collider signals of unparticle physics", *Phys. Rev. Lett.* **99** (2007) 051803, doi:10.1103/PhysRevLett.99.051803, arXiv:0704.2588.
- [37] N. Arkani-Hamed, S. Dimopoulos, and G. R. Dvali, "The hierarchy problem and new dimensions at a millimeter", *Phys. Lett. B* **429** (1998) 263, doi:10.1016/S0370-2693(98)00466-3, arXiv:hep-ph/9803315.
- [38] T. Han, J. D. Lykken, and R. Zhang, "On Kaluza-Klein states from large extra dimensions", *Phys. Rev. D* **59** (1999) 105006, doi:10.1103/PhysRevD.59.105006, arXiv:hep-ph/9811350.
- [39] CMS Collaboration, "The CMS trigger system", *JINST* **12** (2017) P01020, doi:10.1088/1748-0221/12/01/P01020, arXiv:1609.02366.
- [40] CMS Collaboration, "The CMS experiment at the CERN LHC", *JINST* **3** (2008) S08004, doi:10.1088/1748-0221/3/08/S08004.
- [41] O. Mattelaer and E. Vryonidou, "Dark matter production through loop-induced processes at the LHC: the s-channel mediator case", *Eur. Phys. J. C* **75** (2015) 436, doi:10.1140/epjc/s10052-015-3665-5, arXiv:1508.00564.
- [42] M. Neubert, J. Wang, and C. Zhang, "Higher-order QCD predictions for dark matter production in mono-Z searches at the LHC", *JHEP* **02** (2016) 082, doi:10.1007/JHEP02(2016)082, arXiv:1509.05785.
- [43] J. Alwall et al., "The automated computation of tree-level and next-to-leading order differential cross sections, and their matching to parton shower simulations", *JHEP* **07** (2014) 079, doi:10.1007/JHEP07(2014)079, arXiv:1405.0301.
- [44] R. Frederix and S. Frixione, "Merging meets matching in MC@NLO", *JHEP* **12** (2012) 061, doi:10.1007/JHEP12(2012)061, arXiv:1209.6215.
- [45] P. Artoisenet, R. Frederix, O. Mattelaer, and R. Rietkerk, "Automatic spin-entangled decays of heavy resonances in Monte Carlo simulations", *JHEP* **03** (2013) 015, doi:10.1007/JHEP03(2013)015, arXiv:1212.3460.
- [46] J. Alwall et al., "Comparative study of various algorithms for the merging of parton showers and matrix elements in hadronic collisions", *Eur. Phys. J. C* **53** (2008) 473, doi:10.1140/epjc/s10052-007-0490-5, arXiv:0706.2569.
- [47] P. Nason, "A new method for combining NLO QCD with shower Monte Carlo algorithms", *JHEP* **11** (2004) 040, doi:10.1088/1126-6708/2004/11/040, arXiv:hep-ph/0409146.
- [48] S. Frixione, P. Nason, and C. Oleari, "Matching NLO QCD computations with parton shower simulations: the POWHEG method", *JHEP* **11** (2007) 070, doi:10.1088/1126-6708/2007/11/070, arXiv:0709.2092.

- [49] S. Alioli, P. Nason, C. Oleari, and E. Re, “A general framework for implementing NLO calculations in shower Monte Carlo programs: the POWHEG BOX”, *JHEP* **06** (2010) 043, doi:10.1007/JHEP06(2010)043, arXiv:1002.2581.
- [50] S. Frixione, P. Nason, and G. Ridolfi, “A positive-weight next-to-leading-order Monte Carlo for heavy flavour hadroproduction”, *JHEP* **09** (2007) 126, doi:10.1088/1126-6708/2007/09/126, arXiv:0707.3088.
- [51] E. Bagnaschi, G. Degrossi, P. Slavich, and A. Vicini, “Higgs production via gluon fusion in the POWHEG approach in the SM and in the MSSM”, *JHEP* **02** (2012) 088, doi:10.1007/JHEP02(2012)088, arXiv:1111.2854.
- [52] LHC Higgs Cross Section Working Group, “Handbook of LHC Higgs cross sections: 4. deciphering the nature of the Higgs sector”, *CERN* (2016) doi:10.23731/CYRM-2017-002, arXiv:1610.07922.
- [53] T. Sjöstrand et al., “An introduction to PYTHIA 8.2”, *Comput. Phys. Commun.* **191** (2015) 159, doi:10.1016/j.cpc.2015.01.024, arXiv:1410.3012.
- [54] S. Ask et al., “Real emission and virtual exchange of gravitons and unparticles in Pythia8”, *Comput. Phys. Commun.* **181** (2010) 1593, doi:10.1016/j.cpc.2010.05.013, arXiv:0912.4233.
- [55] S. Ask, “Simulation of Z plus graviton/unparticle production at the LHC”, *Eur. Phys. J. C* **60** (2009) 509, doi:10.1140/epjc/s10052-009-0949-7, arXiv:0809.4750.
- [56] NNPDF Collaboration, “Parton distributions from high-precision collider data”, *Eur. Phys. J. C* **77** (2017) 663, doi:10.1140/epjc/s10052-017-5199-5, arXiv:1706.00428.
- [57] CMS Collaboration, “Event generator tunes obtained from underlying event and multiparton scattering measurements”, *Eur. Phys. J. C* **76** (2016) 155, doi:10.1140/epjc/s10052-016-3988-x, arXiv:1512.00815.
- [58] CMS Collaboration, “Extraction and validation of a new set of CMS PYTHIA8 tunes from underlying-event measurements”, *Eur. Phys. J. C* **80** (2020) 4, doi:10.1140/epjc/s10052-019-7499-4, arXiv:1903.12179.
- [59] GEANT4 Collaboration, “GEANT4 — a simulation toolkit”, *Nucl. Instrum. Meth. A* **506** (2003) 250, doi:10.1016/S0168-9002(03)01368-8.
- [60] CMS Collaboration, “Pileup mitigation at CMS in 13 TeV data”, (3, 2020). arXiv:2003.00503. Submitted to JINST.
- [61] CMS Collaboration, “Particle-flow reconstruction and global event description with the CMS detector”, *JINST* **12** (2017) P10003, doi:10.1088/1748-0221/12/10/P10003, arXiv:1706.04965.
- [62] M. Cacciari, G. P. Salam, and G. Soyez, “The anti- k_T jet clustering algorithm”, *JHEP* **04** (2008) 063, doi:10.1088/1126-6708/2008/04/063, arXiv:0802.1189.
- [63] M. Cacciari, G. P. Salam, and G. Soyez, “FastJet user manual”, *Eur. Phys. J. C* **72** (2012) 1896, doi:10.1140/epjc/s10052-012-1896-2, arXiv:1111.6097.

- [64] CMS Collaboration, “Performance of photon reconstruction and identification with the CMS detector in proton-proton collisions at $\sqrt{s} = 8$ TeV”, *JINST* **10** (2015) P08010, doi:10.1088/1748-0221/10/08/P08010, arXiv:1502.02702.
- [65] CMS Collaboration, “Performance of the CMS muon detector and muon reconstruction with proton-proton collisions at $\sqrt{s} = 13$ TeV”, *JINST* **13** (2018) P06015, doi:10.1088/1748-0221/13/06/P06015, arXiv:1804.04528.
- [66] CMS Collaboration, “Jet energy scale and resolution in the CMS experiment in pp collisions at 8 TeV”, *JINST* **12** (2017) P02014, doi:10.1088/1748-0221/12/02/P02014, arXiv:1607.03663.
- [67] CMS Collaboration, “Jet algorithms performance in 13 TeV data”, CMS Physics Analysis Summary CMS-PAS-JME-16-003, 2016.
- [68] CMS Collaboration, “Identification of heavy-flavour jets with the CMS detector in pp collisions at 13 TeV”, *JINST* **13** (2018) P05011, doi:10.1088/1748-0221/13/05/P05011, arXiv:1712.07158.
- [69] CMS Collaboration, “Performance of reconstruction and identification of τ leptons decaying to hadrons and ν_τ in pp collisions at $\sqrt{s} = 13$ TeV”, *JINST* **13** (2018) P10005, doi:10.1088/1748-0221/13/10/P10005, arXiv:1809.02816.
- [70] CMS Collaboration, “Performance of missing transverse momentum reconstruction in proton-proton collisions at $\sqrt{s} = 13$ TeV using the CMS detector”, *JINST* **14** (2019) P07004, doi:10.1088/1748-0221/14/07/P07004, arXiv:1903.06078.
- [71] Particle Data Group, M. Tanabashi et al., “Review of particle physics”, *Phys. Rev. D* **98** (2018) 030001, doi:10.1103/PhysRevD.98.030001.
- [72] CMS Collaboration, “Measurements of the $pp \rightarrow WZ$ inclusive and differential production cross section and constraints on charged anomalous triple gauge couplings at $\sqrt{s} = 13$ TeV”, *JHEP* **04** (2019) 122, doi:10.1007/JHEP04(2019)122, arXiv:1901.03428.
- [73] The ATLAS Collaboration, the CMS Collaboration, and the LHC Higgs Combination Group, “Procedure for the LHC Higgs boson search combination in Summer 2011”, Technical Report CMS-NOTE-2011-005. ATL-PHYS-PUB-2011-11, CERN, Geneva, Aug, 2011.
- [74] CMS Collaboration, “CMS luminosity measurement for the 2016 data-taking period”, CMS Physics Analysis Summary CMS-PAS-LUM-17-001, 2017.
- [75] CMS Collaboration, “CMS luminosity measurement for the 2017 data-taking period at $\sqrt{s} = 13$ TeV”, CMS Physics Analysis Summary CMS-PAS-LUM-17-004, 2017.
- [76] CMS Collaboration, “CMS luminosity measurement for the 2018 data-taking period at $\sqrt{s} = 13$ TeV”, CMS Physics Analysis Summary CMS-PAS-LUM-18-002, 2018.
- [77] CMS Collaboration, “Performance of electron reconstruction and selection with the CMS detector in proton-proton collisions at $\sqrt{s} = 8$ TeV”, *JINST* **10** (2015) P06005, doi:10.1088/1748-0221/10/06/P06005, arXiv:1502.02701.

- [78] CMS Collaboration, “Measurements of differential Z boson production cross sections in proton-proton collisions at $\sqrt{s} = 13$ TeV”, *JHEP* **12** (2019) 061, doi:10.1007/JHEP12(2019)061, arXiv:1909.04133.
- [79] CMS Collaboration, “Measurement of the inelastic proton-proton cross section at $\sqrt{s} = 13$ TeV”, *JHEP* **07** (2018) 161, doi:10.1007/JHEP07(2018)161, arXiv:1802.02613.
- [80] J. Rojo et al., “The PDF4LHC report on PDFs and LHC data: Results from Run I and preparation for Run II”, *J. Phys. G* **42** (2015) 103103, doi:10.1088/0954-3899/42/10/103103, arXiv:1507.00556.
- [81] J. Butterworth et al., “PDF4LHC recommendations for LHC Run II”, *J. Phys. G* **43** (2016) 023001, doi:10.1088/0954-3899/43/2/023001, arXiv:1510.03865.
- [82] A. Accardi et al., “A critical appraisal and evaluation of modern PDFs”, *Eur. Phys. J. C* **76** (2016) 471, doi:10.1140/epjc/s10052-016-4285-4, arXiv:1603.08906.
- [83] A. Bierweiler, T. Kasprzik, and J. H. Kuhn, “Vector-boson pair production at the LHC to $\mathcal{O}(\alpha^3)$ accuracy”, *JHEP* **12** (2013) 071, doi:10.1007/JHEP12(2013)071, arXiv:1305.5402.
- [84] S. Gieseke, T. Kasprzik, and J. H. Kahn, “Vector-boson pair production and electroweak corrections in HERWIG++”, *Eur. Phys. J. C* **74** (2014) 2988, doi:10.1140/epjc/s10052-014-2988-y, arXiv:1401.3964.
- [85] M. Grazzini, S. Kallweit, D. Rathlev, and M. Wiesemann, “ $W^\pm Z$ production at hadron colliders in NNLO QCD”, *Phys. Lett. B* **761** (2016) 179–183, doi:10.1016/j.physletb.2016.08.017, arXiv:1604.08576.
- [86] J. Baglio, L. D. Ninh, and M. M. Weber, “Massive gauge boson pair production at the LHC: a next-to-leading order story”, *Phys. Rev. D* **88** (2013) 113005, doi:10.1103/PhysRevD.88.099902, arXiv:1307.4331. [Erratum: *Phys. Rev. D* **94**, 099902 (2016)].
- [87] M. Grazzini, S. Kallweit, and D. Rathlev, “ZZ production at the LHC: fiducial cross sections and distributions in NNLO QCD”, *Phys. Lett. B* **750** (2015) 407–410, doi:10.1016/j.physletb.2015.09.055, arXiv:1507.06257.
- [88] J. M. Campbell, R. Ellis, and C. Williams, “Vector boson pair production at the LHC”, *JHEP* **07** (2011) 018, doi:10.1007/JHEP07(2011)018, arXiv:1105.0020.
- [89] A. L. Read, “Presentation of search results: the CLs technique”, *J. Phys. G: Nucl. Part. Phys.* **28** (2002) 2693, doi:10.1088/0954-3899/28/10/313.
- [90] T. Junk, “Confidence level computation for combining searches with small statistics”, *Nucl. Instrum. Meth. A* **434** (1999) 435, doi:10.1016/S0168-9002(99)00498-2.
- [91] L. Demortier, “P values and nuisance parameters”, in *Statistical issues for LHC physics. Proceedings, Workshop, PHYSTAT-LHC, Geneva, Switzerland, June 27-29, 2007*, p. 23. 2008. doi:10.5170/CERN-2008-001.
- [92] LHC Dark Matter Working Group, “Recommendations of the LHC Dark Matter Working Group: Comparing LHC searches for dark matter mediators in visible and invisible decay channels and calculations of the thermal relic density”, *Phys. Dark Univ.* **26** (2019) 100377, doi:10.1016/j.dark.2019.100377, arXiv:1703.05703.

- [93] XENON Collaboration, “Dark matter search results from a one ton-year exposure of XENON1T”, *Phys. Rev. Lett.* **121** (2018) 111302, doi:10.1103/PhysRevLett.121.111302, arXiv:1805.12562.
- [94] LUX Collaboration, “Results from a search for dark matter in the complete LUX exposure”, *Phys. Rev. Lett.* **118** (2017) 021303, doi:10.1103/PhysRevLett.118.021303, arXiv:1608.07648.
- [95] PandaX-II Collaboration, “Dark matter results from 54-ton-day exposure of PandaX-II experiment”, *Phys. Rev. Lett.* **119** (2017) 181302, doi:10.1103/PhysRevLett.119.181302, arXiv:1708.06917.
- [96] CRESST Collaboration, “First results from the CRESST-III low-mass dark matter program”, *Phys. Rev. D* **100** (2019) 102002, doi:10.1103/PhysRevD.100.102002, arXiv:1904.00498.
- [97] DarkSide Collaboration, “Low-mass dark matter search with the DarkSide-50 experiment”, *Phys. Rev. Lett.* **121** (2018) 081307, doi:10.1103/PhysRevLett.121.081307, arXiv:1802.06994.
- [98] PICO Collaboration, “Dark matter search results from the complete exposure of the PICO-60 C₃F₈ bubble chamber”, *Phys. Rev. D* **100** (2019) 022001, doi:10.1103/PhysRevD.100.022001, arXiv:1902.04031.
- [99] PICO Collaboration, “Improved dark matter search results from PICO-2L Run 2”, *Phys. Rev. D* **93** (2016) 061101, doi:10.1103/PhysRevD.93.061101, arXiv:1601.03729.
- [100] IceCube Collaboration, “Improved limits on dark matter annihilation in the sun with the 79-string IceCube detector and implications for supersymmetry”, *JCAP* **04** (2016) 022, doi:10.1088/1475-7516/2016/04/022, arXiv:1601.00653.
- [101] Super-Kamiokande Collaboration, “Search for neutrinos from annihilation of captured low-mass dark matter particles in the Sun by Super-Kamiokande”, *Phys. Rev. Lett.* **114** (2015) 141301, doi:10.1103/PhysRevLett.114.141301, arXiv:1503.04858.
- [102] ATLAS Collaboration, “Constraints on mediator-based dark matter and scalar dark energy models using $\sqrt{s} = 13$ TeV pp collision data collected by the ATLAS detector”, *JHEP* **05** (2019) 142, doi:10.1007/JHEP05(2019)142, arXiv:1903.01400.
- [103] LHC Higgs Cross Section Working Group, “Handbook of LHC Higgs Cross Sections: 3. Higgs Properties”, *CERN* (2013) doi:10.5170/CERN-2013-004, arXiv:1307.1347.
- [104] R. V. Harlander, J. Klappert, S. Liebler, and L. Simon, “vh@nnlo-v2: new physics in Higgs strahlung”, *JHEP* **05** (2018) 089, doi:10.1007/JHEP05(2018)089, arXiv:1802.04817.

A The CMS Collaboration

Yerevan Physics Institute, Yerevan, Armenia

A.M. Sirunyan[†], A. Tumasyan

Institut für Hochenergiephysik, Wien, Austria

W. Adam, T. Bergauer, M. Dragicevic, J. Erö, A. Escalante Del Valle, R. Frühwirth¹, M. Jeitler¹, N. Krammer, L. Lechner, D. Liko, T. Madlener, I. Mikulec, F.M. Pitters, N. Rad, J. Schieck¹, R. Schöfbeck, M. Spanring, S. Templ, W. Waltenberger, C.-E. Wulz¹, M. Zarucki

Institute for Nuclear Problems, Minsk, Belarus

V. Chekhovskiy, A. Litomin, V. Makarenko, J. Suarez Gonzalez

Universiteit Antwerpen, Antwerpen, Belgium

M.R. Darwish², E.A. De Wolf, D. Di Croce, X. Janssen, T. Kello³, A. Lelek, M. Pieters, H. Rejeb Sfar, H. Van Haevermaet, P. Van Mechelen, S. Van Putte, N. Van Remortel

Vrije Universiteit Brussel, Brussel, Belgium

F. Blekman, E.S. Bols, S.S. Chhibra, J. D'Hondt, J. De Clercq, D. Lontkovskiy, S. Lowette, I. Marchesini, S. Moortgat, A. Morton, Q. Python, S. Tavernier, W. Van Doninck, P. Van Mulders

Université Libre de Bruxelles, Bruxelles, Belgium

D. Beghin, B. Bilin, B. Clerboux, G. De Lentdecker, B. Dorney, L. Favart, A. Grebenyuk, A.K. Kalsi, I. Makarenko, L. Moureaux, L. Pétré, A. Popov, N. Postiau, E. Starling, L. Thomas, C. Vander Velde, P. Vanlaer, D. Vannerom, L. Wezenbeek

Ghent University, Ghent, Belgium

T. Cornelis, D. Dobur, M. Gruchala, I. Khvastunov⁴, M. Niedziela, C. Roskas, K. Skovpen, M. Tytgat, W. Verbeke, B. Vermassen, M. Vit

Université Catholique de Louvain, Louvain-la-Neuve, Belgium

G. Bruno, F. Bury, C. Caputo, P. David, C. Delaere, M. Delcourt, I.S. Donertas, A. Giammanco, V. Lemaitre, K. Mondal, J. Prisciandaro, A. Taliencio, M. Teklishyn, P. Vischia, S. Wuyckens, J. Zobec

Centro Brasileiro de Pesquisas Fisicas, Rio de Janeiro, Brazil

G.A. Alves, C. Hensel, A. Moraes

Universidade do Estado do Rio de Janeiro, Rio de Janeiro, Brazil

W.L. Aldá Júnior, E. Belchior Batista Das Chagas, H. BRANDAO MALBOUISSON, W. Carvalho, J. Chinellato⁵, E. Coelho, E.M. Da Costa, G.G. Da Silveira⁶, D. De Jesus Damiao, S. Fonseca De Souza, J. Martins⁷, D. Matos Figueiredo, M. Medina Jaime⁸, C. Mora Herrera, L. Mundim, H. Nogima, P. Rebello Teles, L.J. Sanchez Rosas, A. Santoro, S.M. Silva Do Amaral, A. Sznajder, M. Thiel, F. Torres Da Silva De Araujo, A. Vilela Pereira

Universidade Estadual Paulista ^a, Universidade Federal do ABC ^b, São Paulo, Brazil

C.A. Bernardes^{a,a}, L. Calligaris^a, T.R. Fernandez Perez Tomei^a, E.M. Gregores^{a,b}, D.S. Lemos^a, P.G. Mercadante^{a,b}, S.F. Novaes^a, Sandra S. Padula^a

Institute for Nuclear Research and Nuclear Energy, Bulgarian Academy of Sciences, Sofia, Bulgaria

A. Aleksandrov, G. Antchev, I. Atanasov, R. Hadjiiska, P. Iaydjiev, M. Misheva, M. Rodozov, M. Shopova, G. Sultanov

University of Sofia, Sofia, Bulgaria

M. Bonchev, A. Dimitrov, T. Ivanov, L. Litov, B. Pavlov, P. Petkov, A. Petrov

Beihang University, Beijing, ChinaW. Fang³, Q. Guo, H. Wang, L. Yuan**Department of Physics, Tsinghua University, Beijing, China**

M. Ahmad, Z. Hu, Y. Wang

Institute of High Energy Physics, Beijing, ChinaE. Chapon, G.M. Chen⁹, H.S. Chen⁹, M. Chen, A. Kapoor, D. Leggat, H. Liao, Z. Liu, R. Sharma, A. Spiezia, J. Tao, J. Thomas-wilsker, J. Wang, H. Zhang, S. Zhang⁹, J. Zhao**State Key Laboratory of Nuclear Physics and Technology, Peking University, Beijing, China**

A. Agapitos, Y. Ban, C. Chen, Q. Huang, A. Levin, Q. Li, M. Lu, X. Lyu, Y. Mao, S.J. Qian, D. Wang, Q. Wang, J. Xiao

Sun Yat-Sen University, Guangzhou, China

Z. You

Institute of Modern Physics and Key Laboratory of Nuclear Physics and Ion-beam Application (MOE) - Fudan University, Shanghai, ChinaX. Gao³**Zhejiang University, Hangzhou, China**

M. Xiao

Universidad de Los Andes, Bogota, Colombia

C. Avila, A. Cabrera, C. Florez, J. Fraga, A. Sarkar, M.A. Segura Delgado

Universidad de Antioquia, Medellin, Colombia

J. Jaramillo, J. Mejia Guisao, F. Ramirez, J.D. Ruiz Alvarez, C.A. Salazar González, N. Vanegas Arbelaez

University of Split, Faculty of Electrical Engineering, Mechanical Engineering and Naval Architecture, Split, Croatia

D. Giljanovic, N. Godinovic, D. Lelas, I. Puljak, T. Sculac

University of Split, Faculty of Science, Split, Croatia

Z. Antunovic, M. Kovac

Institute Rudjer Boskovic, Zagreb, CroatiaV. Brigljevic, D. Ferencek, D. Majumder, M. Roguljic, A. Starodumov¹⁰, T. Susa**University of Cyprus, Nicosia, Cyprus**

M.W. Ather, A. Attikis, E. Erodou, A. Ioannou, G. Kole, M. Kolosova, S. Konstantinou, G. Mavromanolakis, J. Mousa, C. Nicolaou, F. Ptochos, P.A. Razis, H. Rykaczewski, H. Saka, D. Tsiakkouri

Charles University, Prague, Czech RepublicM. Finger¹¹, M. Finger Jr.¹¹, A. Kveton, J. Tomsa**Escuela Politecnica Nacional, Quito, Ecuador**

E. Ayala

Universidad San Francisco de Quito, Quito, Ecuador

E. Carrera Jarrin

Academy of Scientific Research and Technology of the Arab Republic of Egypt, Egyptian Network of High Energy Physics, Cairo, Egypt

S. Elgammal¹², A. Ellithi Kamel¹³, A. Mohamed¹⁴

Center for High Energy Physics (CHEP-FU), Fayoum University, El-Fayoum, Egypt

A. Lotfy, M.A. Mahmoud

National Institute of Chemical Physics and Biophysics, Tallinn, Estonia

S. Bhowmik, A. Carvalho Antunes De Oliveira, R.K. Dewanjee, K. Ehataht, M. Kadastik, M. Raidal, C. Veelken

Department of Physics, University of Helsinki, Helsinki, Finland

P. Eerola, L. Forthomme, H. Kirschenmann, K. Osterberg, M. Voutilainen

Helsinki Institute of Physics, Helsinki, Finland

E. Brücken, F. Garcia, J. Havukainen, V. Karimäki, M.S. Kim, R. Kinnunen, T. Lampén, K. Lassila-Perini, S. Laurila, S. Lehti, T. Lindén, H. Siikonen, E. Tuominen, J. Tuominiemi

Lappeenranta University of Technology, Lappeenranta, Finland

P. Luukka, T. Tuuva

IRFU, CEA, Université Paris-Saclay, Gif-sur-Yvette, France

C. Amendola, M. Besancon, F. Couderc, M. Dejardin, D. Denegri, J.L. Faure, F. Ferri, S. Ganjour, A. Givernaud, P. Gras, G. Hamel de Monchenault, P. Jarry, B. Lenzi, E. Locci, J. Malcles, J. Rander, A. Rosowsky, M.Ö. Sahin, A. Savoy-Navarro¹⁵, M. Titov, G.B. Yu

Laboratoire Leprince-Ringuet, CNRS/IN2P3, Ecole Polytechnique, Institut Polytechnique de Paris, Paris, France

S. Ahuja, F. Beaudette, M. Bonanomi, A. Buchot Perraguin, P. Busson, C. Charlot, O. Davignon, B. Diab, G. Falmagne, R. Granier de Cassagnac, A. Hakimi, I. Kucher, A. Lobanov, C. Martin Perez, M. Nguyen, C. Ochando, P. Paganini, J. Rembser, R. Salerno, J.B. Sauvan, Y. Sirois, A. Zabi, A. Zghiche

Université de Strasbourg, CNRS, IPHC UMR 7178, Strasbourg, France

J.-L. Agram¹⁶, J. Andrea, D. Bloch, G. Bourgatte, J.-M. Brom, E.C. Chabert, C. Collard, J.-C. Fontaine¹⁶, D. Gelé, U. Goerlach, C. Grimault, A.-C. Le Bihan, P. Van Hove

Université de Lyon, Université Claude Bernard Lyon 1, CNRS-IN2P3, Institut de Physique Nucléaire de Lyon, Villeurbanne, France

E. Asilar, S. Beauceron, C. Bernet, G. Boudoul, C. Camen, A. Carle, N. Chanon, D. Contardo, P. Depasse, H. El Mamouni, J. Fay, S. Gascon, M. Gouzevitch, B. Ille, Sa. Jain, I.B. Laktineh, H. Lattaud, A. Lesauvage, M. Lethuillier, L. Mirabito, L. Torterotot, G. Touquet, M. Vander Donckt, S. Viret

Georgian Technical University, Tbilisi, Georgia

A. Khvedelidze¹¹, Z. Tsamalaidze¹¹

RWTH Aachen University, I. Physikalisches Institut, Aachen, Germany

L. Feld, K. Klein, M. Lipinski, D. Meuser, A. Pauls, M. Preuten, M.P. Rauch, J. Schulz, M. Teroerde

RWTH Aachen University, III. Physikalisches Institut A, Aachen, Germany

D. Eliseev, M. Erdmann, P. Fackeldey, B. Fischer, S. Ghosh, T. Hebbeker, K. Hoepfner, H. Keller, L. Mastrolorenzo, M. Merschmeyer, A. Meyer, G. Mocellin, S. Mondal, S. Mukherjee, D. Noll,

A. Novak, T. Pook, A. Pozdnyakov, T. Quast, Y. Rath, H. Reithler, J. Roemer, A. Schmidt, S.C. Schuler, A. Sharma, S. Wiedenbeck, S. Zaleski

RWTH Aachen University, III. Physikalisches Institut B, Aachen, Germany

C. Dziwok, G. Flügge, W. Haj Ahmad¹⁷, O. Hlushchenko, T. Kress, A. Nowack, C. Pistone, O. Pooth, D. Roy, H. Sert, A. Stahl¹⁸, T. Ziemons

Deutsches Elektronen-Synchrotron, Hamburg, Germany

H. Aarup Petersen, M. Aldaya Martin, P. Asmuss, I. Babounikau, S. Baxter, O. Behnke, A. Bermúdez Martínez, A.A. Bin Anuar, K. Borrás¹⁹, V. Botta, D. Brunner, A. Campbell, A. Cardini, P. Connor, S. Consuegra Rodríguez, V. Danilov, A. De Wit, M.M. Defranchis, L. Didukh, D. Domínguez Damiani, G. Eckerlin, D. Eckstein, T. Eichhorn, L.I. Estevez Banos, E. Gallo²⁰, A. Geiser, A. Giraldi, A. Grohsjean, M. Guthoff, A. Harb, A. Jafari²¹, N.Z. Jomhari, H. Jung, A. Kasem¹⁹, M. Kasemann, H. Kaveh, C. Kleinwort, J. Knolle, D. Krücker, W. Lange, T. Lenz, J. Lidrych, K. Lipka, W. Lohmann²², R. Mankel, I.-A. Melzer-Pellmann, J. Metwally, A.B. Meyer, M. Meyer, M. Missiroli, J. Mnich, A. Mussgiller, V. Myronenko, Y. Otari, D. Pérez Adán, S.K. Pflitsch, D. Pitzl, A. Raspereza, A. Saggio, A. Saibel, M. Savitskyi, V. Scheurer, C. Schwanenberger, A. Singh, R.E. Sosa Ricardo, N. Tonon, O. Turkot, A. Vagnerini, M. Van De Klundert, R. Walsh, D. Walter, Y. Wen, K. Wichmann, C. Wissing, S. Wuchterl, O. Zenaiev, R. Zlebcik

University of Hamburg, Hamburg, Germany

R. Aggleton, S. Bein, L. Benato, A. Benecke, K. De Leo, T. Dreyer, A. Ebrahimi, M. Eich, F. Feindt, A. Fröhlich, C. Garbers, E. Garutti, P. Gunnellini, J. Haller, A. Hinzmann, A. Karavdina, G. Kasieczka, R. Klanner, R. Kogler, V. Kutzner, J. Lange, T. Lange, A. Malara, C.E.N. Niemeyer, A. Nigamova, K.J. Pena Rodriguez, O. Rieger, P. Schleper, S. Schumann, J. Schwandt, D. Schwarz, J. Sonneveld, H. Stadie, G. Steinbrück, B. Vormwald, I. Zoi

Karlsruher Institut fuer Technologie, Karlsruhe, Germany

S. Baur, J. Bechtel, T. Berger, E. Butz, R. Caspart, T. Chwalek, W. De Boer, A. Dierlamm, A. Droll, K. El Morabit, N. Faltermann, K. Flöh, M. Giffels, A. Gottmann, F. Hartmann¹⁸, C. Heidecker, U. Husemann, M.A. Iqbal, I. Katkov²³, P. Keicher, R. Koppenhöfer, S. Maier, M. Metzler, S. Mitra, D. Müller, Th. Müller, M. Musich, G. Quast, K. Rabbertz, J. Rauser, D. Savoie, D. Schäfer, M. Schnepf, M. Schröder, D. Seith, I. Shvetsov, H.J. Simonis, R. Ulrich, M. Wassmer, M. Weber, R. Wolf, S. Wozniowski

Institute of Nuclear and Particle Physics (INPP), NCSR Demokritos, Aghia Paraskevi, Greece

G. Anagnostou, P. Asenov, G. Daskalakis, T. Gerasis, A. Kyriakis, D. Loukas, G. Paspalaki, A. Stakia

National and Kapodistrian University of Athens, Athens, Greece

M. Diamantopoulou, D. Karasavvas, G. Karathanasis, P. Kontaxakis, C.K. Koraka, A. Manousakis-katsikakis, A. Panagiotou, I. Papavergou, N. Saoulidou, K. Theofilatos, K. Vellidis, E. Vourliotis

National Technical University of Athens, Athens, Greece

G. Bakas, K. Kousouris, I. Papakrivopoulos, G. Tsipolitis, A. Zacharopoulou

University of Ioánnina, Ioánnina, Greece

I. Evangelou, C. Foudas, P. Giannelis, P. Katsoulis, P. Kokkas, S. Mallios, K. Manitaras, N. Manthos, I. Papadopoulos, J. Strogas

MTA-ELTE Lendület CMS Particle and Nuclear Physics Group, Eötvös Loránd University, Budapest, Hungary

M. Bartók²⁴, R. Chudasama, M. Csanad, M.M.A. Gadallah²⁵, S. Lökös²⁶, P. Major, K. Mandal, A. Mehta, G. Pasztor, O. Surányi, G.I. Veres

Wigner Research Centre for Physics, Budapest, Hungary

G. Bencze, C. Hajdu, D. Horvath²⁷, F. Sikler, V. Veszpremi, G. Vesztergombi[†]

Institute of Nuclear Research ATOMKI, Debrecen, Hungary

S. Czellar, J. Karancsi²⁴, J. Molnar, Z. Szillasi, D. Teyssier

Institute of Physics, University of Debrecen, Debrecen, Hungary

P. Raics, Z.L. Trocsanyi, B. Ujvari

Eszterhazy Karoly University, Karoly Robert Campus, Gyongyos, Hungary

T. Csorgo, F. Nemes, T. Novak

Indian Institute of Science (IISc), Bangalore, India

S. Choudhury, J.R. Komaragiri, D. Kumar, L. Panwar, P.C. Tiwari

National Institute of Science Education and Research, HBNI, Bhubaneswar, India

S. Bahinipati²⁸, D. Dash, C. Kar, P. Mal, T. Mishra, V.K. Muraleedharan Nair Bindhu, A. Nayak²⁹, D.K. Sahoo²⁸, N. Sur, S.K. Swain

Panjab University, Chandigarh, India

S. Bansal, S.B. Beri, V. Bhatnagar, S. Chauhan, N. Dhingra³⁰, R. Gupta, A. Kaur, S. Kaur, P. Kumari, M. Meena, K. Sandeep, S. Sharma, J.B. Singh, A.K. Viridi

University of Delhi, Delhi, India

A. Ahmed, A. Bhardwaj, B.C. Choudhary, R.B. Garg, M. Gola, S. Keshri, A. Kumar, M. Naimuddin, P. Priyanka, K. Ranjan, A. Shah

Saha Institute of Nuclear Physics, HBNI, Kolkata, India

M. Bharti³¹, R. Bhattacharya, S. Bhattacharya, D. Bhowmik, S. Dutta, S. Ghosh, B. Gomber³², M. Maity³³, S. Nandan, P. Palit, A. Purohit, P.K. Rout, G. Saha, S. Sarkar, M. Sharan, B. Singh³¹, S. Thakur³¹

Indian Institute of Technology Madras, Madras, India

P.K. Behera, S.C. Behera, P. Kalbhor, A. Muhammad, R. Pradhan, P.R. Pujahari, A. Sharma, A.K. Sikdar

Bhabha Atomic Research Centre, Mumbai, India

D. Dutta, V. Kumar, K. Naskar³⁴, P.K. Netrakanti, L.M. Pant, P. Shukla

Tata Institute of Fundamental Research-A, Mumbai, India

T. Aziz, M.A. Bhat, S. Dugad, R. Kumar Verma, G.B. Mohanty, U. Sarkar

Tata Institute of Fundamental Research-B, Mumbai, India

S. Banerjee, S. Bhattacharya, S. Chatterjee, M. Guchait, S. Karmakar, S. Kumar, G. Majumder, K. Mazumdar, S. Mukherjee, D. Roy

Indian Institute of Science Education and Research (IISER), Pune, India

S. Dube, B. Kansal, S. Pandey, A. Rane, A. Rastogi, S. Sharma

Department of Physics, Isfahan University of Technology, Isfahan, Iran

H. Bakhshiansohi³⁵

Institute for Research in Fundamental Sciences (IPM), Tehran, Iran

S. Chenarani³⁶, S.M. Etesami, M. Khakzad, M. Mohammadi Najafabadi

University College Dublin, Dublin, Ireland

M. Felcini, M. Grunewald

INFN Sezione di Bari ^a, Università di Bari ^b, Politecnico di Bari ^c, Bari, Italy

M. Abbrescia^{a,b}, R. Aly^{a,b,37}, C. Aruta^{a,b}, A. Colaleo^a, D. Creanza^{a,c}, N. De Filippis^{a,c}, M. De Palma^{a,b}, A. Di Florio^{a,b}, A. Di Pilato^{a,b}, W. Elmetenawee^{a,b}, L. Fiore^a, A. Gelmi^{a,b}, M. Gul^a, G. Iaselli^{a,c}, M. Ince^{a,b}, S. Lezki^{a,b}, G. Maggi^{a,c}, M. Maggi^a, I. Margjeka^{a,b}, V. Mastrapasqua^{a,b}, J.A. Merlin^a, S. My^{a,b}, S. Nuzzo^{a,b}, A. Pompili^{a,b}, G. Pugliese^{a,c}, A. Ranieri^a, G. Selvaggi^{a,b}, L. Silvestris^a, F.M. Simone^{a,b}, R. Venditti^a, P. Verwilligen^a

INFN Sezione di Bologna ^a, Università di Bologna ^b, Bologna, Italy

G. Abbiendi^a, C. Battilana^{a,b}, D. Bonacorsi^{a,b}, L. Borgonovi^{a,b}, S. Braibant-Giacomelli^{a,b}, R. Campanini^{a,b}, P. Capiluppi^{a,b}, A. Castro^{a,b}, F.R. Cavallo^a, M. Cuffiani^{a,b}, G.M. Dallavalle^a, T. Diotallevi^{a,b}, F. Fabbri^a, A. Fanfani^{a,b}, E. Fontanesi^{a,b}, P. Giacomelli^a, L. Giommi^{a,b}, C. Grandi^a, L. Guiducci^{a,b}, F. Iemmi^{a,b}, S. Lo Meo^{a,38}, S. Marcellini^a, G. Masetti^a, F.L. Navarria^{a,b}, A. Perrotta^a, F. Primavera^{a,b}, A.M. Rossi^{a,b}, T. Rovelli^{a,b}, G.P. Siroli^{a,b}, N. Tosi^a

INFN Sezione di Catania ^a, Università di Catania ^b, Catania, Italy

S. Albergo^{a,b,39}, S. Costa^{a,b}, A. Di Mattia^a, R. Potenza^{a,b}, A. Tricomi^{a,b,39}, C. Tuve^{a,b}

INFN Sezione di Firenze ^a, Università di Firenze ^b, Firenze, Italy

G. Barbagli^a, A. Cassese^a, R. Ceccarelli^{a,b}, V. Ciulli^{a,b}, C. Civinini^a, R. D'Alessandro^{a,b}, F. Fiori^a, E. Focardi^{a,b}, G. Latino^{a,b}, P. Lenzi^{a,b}, M. Lizzo^{a,b}, M. Meschini^a, S. Paoletti^a, R. Seidita^{a,b}, G. Sguazzoni^a, L. Viliani^a

INFN Laboratori Nazionali di Frascati, Frascati, Italy

L. Benussi, S. Bianco, D. Piccolo

INFN Sezione di Genova ^a, Università di Genova ^b, Genova, Italy

M. Bozzo^{a,b}, F. Ferro^a, R. Mulargia^{a,b}, E. Robutti^a, S. Tosi^{a,b}

INFN Sezione di Milano-Bicocca ^a, Università di Milano-Bicocca ^b, Milano, Italy

A. Benaglia^a, A. Beschi^{a,b}, F. Brivio^{a,b}, F. Ceteorelli^{a,b}, V. Ciriolo^{a,b,18}, F. De Guio^{a,b}, M.E. Dinardo^{a,b}, P. Dini^a, S. Gennai^a, A. Ghezzi^{a,b}, P. Govoni^{a,b}, L. Guzzi^{a,b}, M. Malberti^a, S. Malvezzi^a, D. Menasce^a, F. Monti^{a,b}, L. Moroni^a, M. Paganoni^{a,b}, D. Pedrini^a, S. Ragazzi^{a,b}, T. Tabarelli de Fatis^{a,b}, D. Valsecchi^{a,b,18}, D. Zuolo^{a,b}

INFN Sezione di Napoli ^a, Università di Napoli 'Federico II' ^b, Napoli, Italy, Università della Basilicata ^c, Potenza, Italy, Università G. Marconi ^d, Roma, Italy

S. Buontempo^a, N. Cavallo^{a,c}, A. De Iorio^{a,b}, F. Fabozzi^{a,c}, F. Fienga^a, A.O.M. Iorio^{a,b}, L. Lista^{a,b}, S. Meola^{a,d,18}, P. Paolucci^{a,18}, B. Rossi^a, C. Sciacca^{a,b}, E. Voevodina^{a,b}

INFN Sezione di Padova ^a, Università di Padova ^b, Padova, Italy, Università di Trento ^c, Trento, Italy

P. Azzi^a, N. Bacchetta^a, D. Bisello^{a,b}, A. Boletti^{a,b}, A. Bragagnolo^{a,b}, R. Carlin^{a,b}, P. Checchia^a, P. De Castro Manzano^a, T. Dorigo^a, F. Gasparini^{a,b}, U. Gasparini^{a,b}, S.Y. Hoh^{a,b}, L. Layer^{a,40}, M. Margoni^{a,b}, A.T. Meneguzzo^{a,b}, M. Presilla^{a,b}, P. Ronchese^{a,b}, R. Rossin^{a,b}, F. Simonetto^{a,b}, G. Strong^a, A. Tiko^a, M. Tosi^{a,b}, H. YARAR^{a,b}, M. Zanetti^{a,b}, P. Zotto^{a,b}, A. Zucchetta^{a,b}, G. Zumerle^{a,b}

INFN Sezione di Pavia ^a, Università di Pavia ^b, Pavia, Italy

C. Aime^{a,b}, A. Braghieri^a, S. Calzaferri^{a,b}, D. Fiorina^{a,b}, P. Montagna^{a,b}, S.P. Ratti^{a,b}, V. Re^a, M. Ressegotti^{a,b}, C. Riccardi^{a,b}, P. Salvini^a, I. Vai^a, P. Vitulo^{a,b}

INFN Sezione di Perugia ^a, Università di Perugia ^b, Perugia, Italy

M. Biasini^{a,b}, G.M. Bilei^a, D. Ciangottini^{a,b}, L. Fanò^{a,b}, P. Lariccia^{a,b}, G. Mantovani^{a,b}, V. Mariani^{a,b}, M. Menichelli^a, F. Moscatelli^a, A. Piccinelli^{a,b}, A. Rossi^{a,b}, A. Santocchia^{a,b}, D. Spiga^a, T. Tedeschi^{a,b}

INFN Sezione di Pisa ^a, Università di Pisa ^b, Scuola Normale Superiore di Pisa ^c, Pisa, Italy

K. Androsov^a, P. Azzurri^a, G. Bagliesi^a, V. Bertacchi^{a,c}, L. Bianchini^a, T. Boccali^a, R. Castaldi^a, M.A. Ciocci^{a,b}, R. Dell'Orso^a, M.R. Di Domenico^{a,b}, S. Donato^a, L. Giannini^{a,c}, A. Giassi^a, M.T. Grippo^a, F. Ligabue^{a,c}, E. Manca^{a,c}, G. Mandorli^{a,c}, A. Messineo^{a,b}, F. Palla^a, G. Ramirez-Sanchez^{a,c}, A. Rizzi^{a,b}, G. Rolandi^{a,c}, S. Roy Chowdhury^{a,c}, A. Scribano^a, N. Shafiei^{a,b}, P. Spagnolo^a, R. Tenchini^a, G. Tonelli^{a,b}, N. Turini^a, A. Venturi^a, P.G. Verdini^a

INFN Sezione di Roma ^a, Sapienza Università di Roma ^b, Rome, Italy

F. Cavallari^a, M. Cipriani^{a,b}, D. Del Re^{a,b}, E. Di Marco^a, M. Diemoz^a, E. Longo^{a,b}, P. Meridiani^a, G. Organtini^{a,b}, F. Pandolfi^a, R. Paramatti^{a,b}, C. Quaranta^{a,b}, S. Rahatlou^{a,b}, C. Rovelli^a, F. Santanastasio^{a,b}, L. Soffi^{a,b}, R. Tramontano^{a,b}

INFN Sezione di Torino ^a, Università di Torino ^b, Torino, Italy, Università del Piemonte Orientale ^c, Novara, Italy

N. Amapane^{a,b}, R. Arcidiacono^{a,c}, S. Argiro^{a,b}, M. Arneodo^{a,c}, N. Bartosik^a, R. Bellan^{a,b}, A. Bellora^{a,b}, C. Biino^a, A. Cappati^{a,b}, N. Cartiglia^a, S. Cometti^a, M. Costa^{a,b}, R. Covarelli^{a,b}, N. Demaria^a, B. Kiani^{a,b}, F. Legger^a, C. Mariotti^a, S. Maselli^a, E. Migliore^{a,b}, V. Monaco^{a,b}, E. Monteil^{a,b}, M. Monteno^a, M.M. Obertino^{a,b}, G. Ortona^a, L. Pacher^{a,b}, N. Pastrone^a, M. Pelliccioni^a, G.L. Pinna Angioni^{a,b}, M. Ruspa^{a,c}, R. Salvatico^{a,b}, F. Siviero^{a,b}, V. Sola^a, A. Solano^{a,b}, D. Soldi^{a,b}, A. Staiano^a, D. Trocino^{a,b}

INFN Sezione di Trieste ^a, Università di Trieste ^b, Trieste, Italy

S. Belforte^a, V. Candelise^{a,b}, M. Casarsa^a, F. Cossutti^a, A. Da Rold^{a,b}, G. Della Ricca^{a,b}, F. Vazzoler^{a,b}

Kyungpook National University, Daegu, Korea

S. Dogra, C. Huh, B. Kim, D.H. Kim, G.N. Kim, J. Lee, S.W. Lee, C.S. Moon, Y.D. Oh, S.I. Pak, B.C. Radburn-Smith, S. Sekmen, Y.C. Yang

Chonnam National University, Institute for Universe and Elementary Particles, Kwangju, Korea

H. Kim, D.H. Moon

Hanyang University, Seoul, Korea

B. Francois, T.J. Kim, J. Park

Korea University, Seoul, Korea

S. Cho, S. Choi, Y. Go, S. Ha, B. Hong, K. Lee, K.S. Lee, J. Lim, J. Park, S.K. Park, J. Yoo

Kyung Hee University, Department of Physics, Seoul, Republic of Korea

J. Goh, A. Gurtu

Sejong University, Seoul, Korea

H.S. Kim, Y. Kim

Seoul National University, Seoul, Korea

J. Almond, J.H. Bhyun, J. Choi, S. Jeon, J. Kim, J.S. Kim, S. Ko, H. Kwon, H. Lee, K. Lee, S. Lee, K. Nam, B.H. Oh, M. Oh, S.B. Oh, H. Seo, U.K. Yang, I. Yoon

University of Seoul, Seoul, Korea

D. Jeon, J.H. Kim, B. Ko, J.S.H. Lee, I.C. Park, Y. Roh, D. Song, I.J. Watson

Yonsei University, Department of Physics, Seoul, Korea

H.D. Yoo

Sungkyunkwan University, Suwon, Korea

Y. Choi, C. Hwang, Y. Jeong, H. Lee, Y. Lee, I. Yu

Riga Technical University, Riga, Latvia

V. Veckalns⁴¹

Vilnius University, Vilnius, Lithuania

A. Juodagalvis, A. Rinkevicius, G. Tamulaitis

National Centre for Particle Physics, Universiti Malaya, Kuala Lumpur, Malaysia

W.A.T. Wan Abdullah, M.N. Yusli, Z. Zolkapli

Universidad de Sonora (UNISON), Hermosillo, Mexico

J.F. Benitez, A. Castaneda Hernandez, J.A. Murillo Quijada, L. Valencia Palomo

Centro de Investigacion y de Estudios Avanzados del IPN, Mexico City, Mexico

G. Ayala, H. Castilla-Valdez, E. De La Cruz-Burelo, I. Heredia-De La Cruz⁴², R. Lopez-Fernandez, C.A. Mondragon Herrera, D.A. Perez Navarro, A. Sanchez-Hernandez

Universidad Iberoamericana, Mexico City, Mexico

S. Carrillo Moreno, C. Oropeza Barrera, M. Ramirez-Garcia, F. Vazquez Valencia

Benemerita Universidad Autonoma de Puebla, Puebla, Mexico

J. Eysermans, I. Pedraza, H.A. Salazar Ibarquen, C. Uribe Estrada

Universidad Autónoma de San Luis Potosí, San Luis Potosí, Mexico

A. Morelos Pineda

University of Montenegro, Podgorica, Montenegro

J. Mijuskovic⁴, N. Raicevic

University of Auckland, Auckland, New Zealand

D. Krofcheck

University of Canterbury, Christchurch, New Zealand

S. Bheesette, P.H. Butler

National Centre for Physics, Quaid-I-Azam University, Islamabad, Pakistan

A. Ahmad, M.I. Asghar, M.I.M. Awan, H.R. Hoorani, W.A. Khan, M.A. Shah, M. Shoaib, M. Waqas

AGH University of Science and Technology Faculty of Computer Science, Electronics and Telecommunications, Krakow, Poland

V. Avati, L. Grzanka, M. Malawski

National Centre for Nuclear Research, Swierk, Poland

H. Bialkowska, M. Bluj, B. Boimska, T. Frueboes, M. Górski, M. Kazana, M. Szleper, P. Traczyk, P. Zalewski

Institute of Experimental Physics, Faculty of Physics, University of Warsaw, Warsaw, Poland
K. Bunkowski, A. Byszuk⁴³, K. Doroba, A. Kalinowski, M. Konecki, J. Krolikowski, M. Olszewski, M. Walczak

Laboratório de Instrumentação e Física Experimental de Partículas, Lisboa, Portugal
M. Araujo, P. Bargassa, D. Bastos, P. Faccioli, M. Gallinaro, J. Hollar, N. Leonardo, T. Niknejad, J. Seixas, K. Shchelina, O. Toldaiev, J. Varela

Joint Institute for Nuclear Research, Dubna, Russia
S. Afanasiev, P. Bunin, M. Gavrilenko, I. Golutvin, I. Gorbunov, A. Kamenev, V. Karjavine, A. Lanev, A. Malakhov, V. Matveev^{44,45}, P. Moisenz, V. Palichik, V. Perelygin, M. Savina, D. Seitova, V. Shalaev, S. Shmatov, S. Shulha, V. Smirnov, O. Teryaev, N. Voytishin, A. Zarubin, I. Zhizhin

Petersburg Nuclear Physics Institute, Gatchina (St. Petersburg), Russia
G. Gavrillov, V. Golovtsov, Y. Ivanov, V. Kim⁴⁶, E. Kuznetsova⁴⁷, V. Murzin, V. Oreshkin, I. Smirnov, D. Sosnov, V. Sulimov, L. Uvarov, S. Volkov, A. Vorobyev

Institute for Nuclear Research, Moscow, Russia
Yu. Andreev, A. Dermenev, S. Gninenko, N. Golubev, A. Karneyeu, M. Kirsanov, N. Krasnikov, A. Pashenkov, G. Pivovarov, D. Tlisov[†], A. Toropin

Institute for Theoretical and Experimental Physics named by A.I. Alikhanov of NRC 'Kurchatov Institute', Moscow, Russia
V. Epshteyn, V. Gavrillov, N. Lychkovskaya, A. Nikitenko⁴⁸, V. Popov, G. Safronov, A. Spiridonov, A. Stepenov, M. Toms, E. Vlasov, A. Zhokin

Moscow Institute of Physics and Technology, Moscow, Russia
T. Aushev

National Research Nuclear University 'Moscow Engineering Physics Institute' (MEPhI), Moscow, Russia
R. Chistov⁴⁹, M. Danilov⁵⁰, P. Parygin, D. Philippov, S. Polikarpov⁴⁹

P.N. Lebedev Physical Institute, Moscow, Russia
V. Andreev, M. Azarkin, I. Dremin, M. Kirakosyan, A. Terkulov

Skobeltsyn Institute of Nuclear Physics, Lomonosov Moscow State University, Moscow, Russia
A. Belyaev, E. Boos, V. Bunichev, M. Dubinin⁵¹, L. Dudko, A. Ershov, A. Gribushin, V. Klyukhin, O. Kodolova, I. Lokhtin, S. Obraztsov, M. Perfilov, V. Savrin

Novosibirsk State University (NSU), Novosibirsk, Russia
V. Blinov⁵², T. Dimova⁵², L. Kardapoltsev⁵², I. Ovtin⁵², Y. Skovpen⁵²

Institute for High Energy Physics of National Research Centre 'Kurchatov Institute', Protvino, Russia
I. Azhgirey, I. Bayshev, V. Kachanov, A. Kalinin, D. Konstantinov, V. Petrov, R. Ryutin, A. Sobol, S. Troshin, N. Tyurin, A. Uzunian, A. Volkov

National Research Tomsk Polytechnic University, Tomsk, Russia
A. Babaev, A. Iuzhakov, V. Okhotnikov, L. Sukhikh

Tomsk State University, Tomsk, Russia
V. Borchsh, V. Ivanchenko, E. Tcherniaev

University of Belgrade: Faculty of Physics and VINCA Institute of Nuclear Sciences, Belgrade, Serbia

P. Adzic⁵³, P. Cirkovic, M. Dordevic, P. Milenovic, J. Milosevic

Centro de Investigaciones Energéticas Medioambientales y Tecnológicas (CIEMAT), Madrid, Spain

M. Aguilar-Benitez, J. Alcaraz Maestre, A. Álvarez Fernández, I. Bachiller, M. Barrio Luna, Cristina F. Bedoya, J.A. Brochero Cifuentes, C.A. Carrillo Montoya, M. Cepeda, M. Cerrada, N. Colino, B. De La Cruz, A. Delgado Peris, J.P. Fernández Ramos, J. Flix, M.C. Fouz, A. García Alonso, O. Gonzalez Lopez, S. Goy Lopez, J.M. Hernandez, M.I. Josa, J. León Holgado, D. Moran, Á. Navarro Tobar, A. Pérez-Calero Yzquierdo, J. Puerta Pelayo, I. Redondo, L. Romero, S. Sánchez Navas, M.S. Soares, A. Triossi, L. Urda Gómez, C. Willmott

Universidad Autónoma de Madrid, Madrid, Spain

C. Albajar, J.F. de Trocóniz, R. Reyes-Almanza

Universidad de Oviedo, Instituto Universitario de Ciencias y Tecnologías Espaciales de Asturias (ICTEA), Oviedo, Spain

B. Alvarez Gonzalez, J. Cuevas, C. Erice, J. Fernandez Menendez, S. Folgueras, I. Gonzalez Caballero, E. Palencia Cortezon, C. Ramón Álvarez, J. Ripoll Sau, V. Rodríguez Bouza, S. Sanchez Cruz, A. Trapote

Instituto de Física de Cantabria (IFCA), CSIC-Universidad de Cantabria, Santander, Spain

I.J. Cabrillo, A. Calderon, B. Chazin Quero, J. Duarte Campderros, M. Fernandez, P.J. Fernández Manteca, G. Gomez, C. Martinez Rivero, P. Martinez Ruiz del Arbol, F. Matorras, J. Piedra Gomez, C. Prieels, F. Ricci-Tam, T. Rodrigo, A. Ruiz-Jimeno, L. Scodellaro, I. Vila, J.M. Vizan Garcia

University of Colombo, Colombo, Sri Lanka

MK Jayananda, B. Kailasapathy⁵⁴, D.U.J. Sonnadara, DDC Wickramarathna

University of Ruhuna, Department of Physics, Matara, Sri Lanka

W.G.D. Dharmaratna, K. Liyanage, N. Perera, N. Wickramage

CERN, European Organization for Nuclear Research, Geneva, Switzerland

T.K. Aarrestad, D. Abbaneo, B. Akgun, E. Auffray, G. Auzinger, J. Baechler, P. Baillon, A.H. Ball, D. Barney, J. Bendavid, N. Beni, M. Bianco, A. Bocci, P. Bortignon, E. Bossini, E. Brondolin, T. Camporesi, G. Cerminara, L. Cristella, D. d'Enterria, A. Dabrowski, N. Daci, V. Daponte, A. David, A. De Roeck, M. Deile, R. Di Maria, M. Dobson, M. Dünser, N. Dupont, A. Elliott-Peisert, N. Emriskova, F. Fallavollita⁵⁵, D. Fasanella, S. Fiorendi, A. Florent, G. Franzoni, J. Fulcher, W. Funk, S. Giani, D. Gigi, K. Gill, F. Glege, L. Gouskos, M. Guilbaud, D. Gulhan, M. Haranko, J. Hegeman, Y. Iiyama, V. Innocente, T. James, P. Janot, J. Kaspar, J. Kieseler, M. Komm, N. Kratochwil, C. Lange, P. Lecoq, K. Long, C. Lourenço, L. Malgeri, M. Mannelli, A. Massironi, F. Meijers, S. Mersi, E. Meschi, F. Moortgat, M. Mulders, J. Ngadiuba, J. Niedziela, S. Orfanelli, L. Orsini, F. Pantaleo¹⁸, L. Pape, E. Perez, M. Peruzzi, A. Petrilli, G. Petrucciani, A. Pfeiffer, M. Pierini, D. Rabaday, A. Racz, M. Rieger, M. Rovere, H. Sakulin, J. Salfeld-Nebgen, S. Scarfi, C. Schäfer, C. Schwick, M. Selvaggi, A. Sharma, P. Silva, W. Snoeys, P. Sphicas⁵⁶, J. Steggemann, S. Summers, V.R. Tavolaro, D. Treille, A. Tsirou, G.P. Van Onsem, A. Vartak, M. Verzetti, K.A. Wozniak, W.D. Zeuner

Paul Scherrer Institut, Villigen, Switzerland

L. Caminada⁵⁷, W. Erdmann, R. Horisberger, Q. Ingram, H.C. Kaestli, D. Kotlinski, U. Langenegger, T. Rohe

ETH Zurich - Institute for Particle Physics and Astrophysics (IPA), Zurich, Switzerland

M. Backhaus, P. Berger, A. Calandri, N. Chernyavskaya, A. De Cosa, G. Dissertori, M. Dittmar, M. Donegà, C. Dorfer, T. Gadek, T.A. Gómez Espinosa, C. Grab, D. Hits, W. Luster, M. Lyon, R.A. Manzoni, M.T. Meinhard, F. Micheli, F. Nessi-Tedaldi, F. Pauss, V. Perovic, G. Perrin, L. Perrozzi, S. Pigazzini, M.G. Ratti, M. Reichmann, C. Reissel, T. Reitenspiess, B. Ristic, D. Ruini, D.A. Sanz Becerra, M. Schönenberger, V. Stampf, M.L. Vesterbacka Olsson, R. Wallny, D.H. Zhu

Universität Zürich, Zurich, Switzerland

C. AMSLER⁵⁸, C. Botta, D. Brzhechko, M.F. Canelli, R. Del Burgo, J.K. Heikkilä, M. Huwiler, A. Jofrehei, B. Kilminster, S. Leontsinis, A. Macchiolo, P. Meiring, V.M. Mikuni, U. Molinatti, I. Neutelings, G. Rauco, A. Reimers, P. Robmann, K. Schweiger, Y. Takahashi, S. Wertz

National Central University, Chung-Li, Taiwan

C. Adloff⁵⁹, C.M. Kuo, W. Lin, A. Roy, T. Sarkar³³, S.S. Yu

National Taiwan University (NTU), Taipei, Taiwan

L. Ceard, P. Chang, Y. Chao, K.F. Chen, P.H. Chen, W.-S. Hou, Y.y. Li, R.-S. Lu, E. Paganis, A. Psallidas, A. Steen, E. Yazgan

Chulalongkorn University, Faculty of Science, Department of Physics, Bangkok, Thailand

B. Asavapibhop, C. Asawatangtrakuldee, N. Srimanobhas

Çukurova University, Physics Department, Science and Art Faculty, Adana, Turkey

F. Boran, S. Damarcekin⁶⁰, Z.S. Demiroglu, F. Dolek, C. Dozen⁶¹, I. Dumanoglu⁶², E. Eskut, G. Gokbulut, Y. Guler, E. Gurpinar Guler⁶³, I. Hos⁶⁴, C. Isik, E.E. Kangal⁶⁵, O. Kara, A. Kayis Topaksu, U. Kiminsu, G. Onengut, K. Ozdemir⁶⁶, A. Polatoz, A.E. Simsek, B. Tali⁶⁷, U.G. Tok, S. Turkcapar, I.S. Zorbakir, C. Zorbilmez

Middle East Technical University, Physics Department, Ankara, Turkey

B. Isildak⁶⁸, G. Karapinar⁶⁹, K. Ocalan⁷⁰, M. Yalvac⁷¹

Bogazici University, Istanbul, Turkey

I.O. Atakisi, E. Gülmez, M. Kaya⁷², O. Kaya⁷³, Ö. Özçelik, S. Tekten⁷⁴, E.A. Yetkin⁷⁵

Istanbul Technical University, Istanbul, Turkey

A. Cakir, K. Cankocak⁶², Y. Komurcu, S. Sen⁷⁶

Istanbul University, Istanbul, Turkey

F. Aydogmus Sen, S. Cerci⁶⁷, B. Kaynak, S. Ozkorucuklu, D. Sunar Cerci⁶⁷

Institute for Scintillation Materials of National Academy of Science of Ukraine, Kharkov, Ukraine

B. Grynyov

National Scientific Center, Kharkov Institute of Physics and Technology, Kharkov, Ukraine

L. Levchuk

University of Bristol, Bristol, United Kingdom

E. Bhal, S. Bologna, J.J. Brooke, E. Clement, D. Cussans, H. Flacher, J. Goldstein, G.P. Heath, H.F. Heath, L. Kreczko, B. Krikler, S. Paramesvaran, T. Sakuma, S. Seif El Nasr-Storey, V.J. Smith, J. Taylor, A. Titterton

Rutherford Appleton Laboratory, Didcot, United Kingdom

K.W. Bell, A. Belyaev⁷⁷, C. Brew, R.M. Brown, D.J.A. Cockerill, K.V. Ellis, K. Harder,

S. Harper, J. Linacre, K. Manolopoulos, D.M. Newbold, E. Olaiya, D. Petyt, T. Reis, T. Schuh, C.H. Shepherd-Themistocleous, A. Thea, I.R. Tomalin, T. Williams

Imperial College, London, United Kingdom

R. Bainbridge, P. Bloch, S. Bonomally, J. Borg, S. Breeze, O. Buchmuller, A. Bundock, V. Cepaitis, G.S. Chahal⁷⁸, D. Colling, P. Dauncey, G. Davies, M. Della Negra, G. Fedi, G. Hall, G. Iles, J. Langford, L. Lyons, A.-M. Magnan, S. Malik, A. Martelli, V. Milosevic, J. Nash⁷⁹, V. Palladino, M. Pesaresi, D.M. Raymond, A. Richards, A. Rose, E. Scott, C. Seez, A. Shtipliyski, M. Stoye, A. Tapper, K. Uchida, T. Virdee¹⁸, N. Wardle, S.N. Webb, D. Winterbottom, A.G. Zecchinelli

Brunel University, Uxbridge, United Kingdom

J.E. Cole, P.R. Hobson, A. Khan, P. Kyberd, C.K. Mackay, I.D. Reid, L. Teodorescu, S. Zahid

Baylor University, Waco, USA

A. Brinkerhoff, K. Call, B. Caraway, J. Dittmann, K. Hatakeyama, A.R. Kanuganti, C. Madrid, B. McMaster, N. Pastika, S. Sawant, C. Smith, J. Wilson

Catholic University of America, Washington, DC, USA

R. Bartek, A. Dominguez, R. Uniyal, A.M. Vargas Hernandez

The University of Alabama, Tuscaloosa, USA

A. Buccilli, O. Charaf, S.I. Cooper, S.V. Gleyzer, C. Henderson, P. Rumerio, C. West

Boston University, Boston, USA

A. Akpınar, A. Albert, D. Arcaro, C. Cosby, Z. Demiragli, D. Gastler, J. Rohlf, K. Salyer, D. Sperka, D. Spitzbart, I. Suarez, S. Yuan, D. Zou

Brown University, Providence, USA

G. Benelli, B. Burkle, X. Coubez¹⁹, D. Cutts, Y.t. Duh, M. Hadley, U. Heintz, J.M. Hogan⁸⁰, K.H.M. Kwok, E. Laird, G. Landsberg, K.T. Lau, J. Lee, M. Narain, S. Sagir⁸¹, R. Syarif, E. Usai, W.Y. Wong, D. Yu, W. Zhang

University of California, Davis, Davis, USA

R. Band, C. Brainerd, R. Breedon, M. Calderon De La Barca Sanchez, M. Chertok, J. Conway, R. Conway, P.T. Cox, R. Erbacher, C. Flores, G. Funk, F. Jensen, W. Ko[†], O. Kukral, R. Lander, M. Mulhearn, D. Pellett, J. Pilot, M. Shi, D. Taylor, K. Tos, M. Tripathi, Y. Yao, F. Zhang

University of California, Los Angeles, USA

M. Bachtis, R. Cousins, A. Dasgupta, D. Hamilton, J. Hauser, M. Ignatenko, T. Lam, N. Mccoll, W.A. Nash, S. Regnard, D. Saltzberg, C. Schnaible, B. Stone, V. Valuev

University of California, Riverside, Riverside, USA

K. Burt, Y. Chen, R. Clare, J.W. Gary, S.M.A. Ghiasi Shirazi, G. Hanson, G. Karapostoli, O.R. Long, N. Manganeli, M. Olmedo Negrete, M.I. Paneva, W. Si, S. Wimpenny, Y. Zhang

University of California, San Diego, La Jolla, USA

J.G. Branson, P. Chang, S. Cittolin, S. Cooperstein, N. Deelen, J. Duarte, R. Gerosa, D. Gilbert, V. Krutelyov, J. Letts, M. Masciovecchio, S. May, S. Padhi, M. Pieri, V. Sharma, M. Tadel, F. Würthwein, A. Yagil

University of California, Santa Barbara - Department of Physics, Santa Barbara, USA

N. Amin, C. Campagnari, M. Citron, A. Dorsett, V. Dutta, J. Incandela, B. Marsh, H. Mei, A. Ovcharova, H. Qu, M. Quinnan, J. Richman, U. Sarica, D. Stuart, S. Wang

California Institute of Technology, Pasadena, USA

D. Anderson, A. Bornheim, O. Cerri, I. Dutta, J.M. Lawhorn, N. Lu, J. Mao, H.B. Newman, T.Q. Nguyen, J. Pata, M. Spiropulu, J.R. Vlimant, S. Xie, Z. Zhang, R.Y. Zhu

Carnegie Mellon University, Pittsburgh, USA

J. Alison, M.B. Andrews, T. Ferguson, T. Mudholkar, M. Paulini, M. Sun, I. Vorobiev

University of Colorado Boulder, Boulder, USA

J.P. Cumalat, W.T. Ford, E. MacDonald, T. Mulholland, R. Patel, A. Perloff, K. Stenson, K.A. Ulmer, S.R. Wagner

Cornell University, Ithaca, USA

J. Alexander, Y. Cheng, J. Chu, D.J. Cranshaw, A. Datta, A. Frankenthal, K. Mcdermott, J. Monroy, J.R. Patterson, D. Quach, A. Ryd, W. Sun, S.M. Tan, Z. Tao, J. Thom, P. Wittich, M. Zientek

Fermi National Accelerator Laboratory, Batavia, USA

S. Abdullin, M. Albrow, M. Alyari, G. Apollinari, A. Apresyan, A. Apyan, S. Banerjee, L.A.T. Bauerdick, A. Beretvas, D. Berry, J. Berryhill, P.C. Bhat, K. Burkett, J.N. Butler, A. Canepa, G.B. Cerati, H.W.K. Cheung, F. Chlebana, M. Cremonesi, V.D. Elvira, J. Freeman, Z. Gecse, E. Gottschalk, L. Gray, D. Green, S. Grünendahl, O. Gutsche, R.M. Harris, S. Hasegawa, R. Heller, T.C. Herwig, J. Hirschauer, B. Jayatilaka, S. Jindariani, M. Johnson, U. Joshi, P. Klabbers, T. Klijnsma, B. Klima, M.J. Kortelainen, S. Lammel, D. Lincoln, R. Lipton, M. Liu, T. Liu, J. Lykken, K. Maeshima, D. Mason, P. McBride, P. Merkel, S. Mrenna, S. Nahn, V. O'Dell, V. Papadimitriou, K. Pedro, C. Pena⁵¹, O. Prokofyev, F. Ravera, A. Reinsvold Hall, L. Ristori, B. Schneider, E. Sexton-Kennedy, N. Smith, A. Soha, W.J. Spalding, L. Spiegel, S. Stoynev, J. Strait, L. Taylor, S. Tkaczyk, N.V. Tran, L. Uplegger, E.W. Vaandering, H.A. Weber, A. Woodard

University of Florida, Gainesville, USA

D. Acosta, P. Avery, D. Bourilkov, L. Cadamuro, V. Cherepanov, F. Errico, R.D. Field, D. Guerrero, B.M. Joshi, M. Kim, J. Konigsberg, A. Korytov, K.H. Lo, K. Matchev, N. Menendez, G. Mitselmakher, D. Rosenzweig, K. Shi, J. Wang, S. Wang, X. Zuo

Florida State University, Tallahassee, USA

T. Adams, A. Askew, D. Diaz, R. Habibullah, S. Hagopian, V. Hagopian, K.F. Johnson, R. Khurana, T. Kolberg, G. Martinez, H. Prosper, C. Schiber, R. Yohay, J. Zhang

Florida Institute of Technology, Melbourne, USA

M.M. Baarmand, S. Butalla, T. Elkafrawy⁸², M. Hohlmann, D. Noonan, M. Rahmani, M. Saunders, F. Yumiceva

University of Illinois at Chicago (UIC), Chicago, USA

M.R. Adams, L. Apanasevich, H. Becerril Gonzalez, R. Cavanaugh, X. Chen, S. Dittmer, O. Evdokimov, C.E. Gerber, D.A. Hangal, D.J. Hofman, C. Mills, G. Oh, T. Roy, M.B. Tonjes, N. Varelas, J. Viinikainen, X. Wang, Z. Wu

The University of Iowa, Iowa City, USA

M. Alhousseini, K. Dilsiz⁸³, S. Durgut, R.P. Gandrajula, M. Haytmyradov, V. Khristenko, O.K. Köseyan, J.-P. Merlo, A. Mestvirishvili⁸⁴, A. Moeller, J. Nachtman, H. Ogul⁸⁵, Y. Onel, F. Ozok⁸⁶, A. Penzo, C. Snyder, E. Tiras, J. Wetzel, K. Yi⁸⁷

Johns Hopkins University, Baltimore, USA

O. Amram, B. Blumenfeld, L. Corcodilos, M. Eminizer, A.V. Gritsan, S. Kyriacou, P. Maksimovic, C. Mantilla, J. Roskes, M. Swartz, T.Á. Vámi

The University of Kansas, Lawrence, USA

C. Baldenegro Barrera, P. Baringer, A. Bean, A. Bylinkin, T. Isidori, S. Khalil, J. King, G. Krintiras, A. Kropivnitskaya, C. Lindsey, N. Minafra, M. Murray, C. Rogan, C. Royon, S. Sanders, E. Schmitz, J.D. Tapia Takaki, Q. Wang, J. Williams, G. Wilson

Kansas State University, Manhattan, USA

S. Duric, A. Ivanov, K. Kaadze, D. Kim, Y. Maravin, T. Mitchell, A. Modak, A. Mohammadi

Lawrence Livermore National Laboratory, Livermore, USA

F. Rebasoo, D. Wright

University of Maryland, College Park, USA

E. Adams, A. Baden, O. Baron, A. Belloni, S.C. Eno, Y. Feng, N.J. Hadley, S. Jabeen, G.Y. Jeng, R.G. Kellogg, T. Koeth, A.C. Mignerey, S. Nabili, M. Seidel, A. Skuja, S.C. Tonwar, L. Wang, K. Wong

Massachusetts Institute of Technology, Cambridge, USA

D. Abercrombie, B. Allen, R. Bi, S. Brandt, W. Busza, I.A. Cali, Y. Chen, M. D'Alfonso, G. Gomez Ceballos, M. Goncharov, P. Harris, D. Hsu, M. Hu, M. Klute, D. Kovalskyi, J. Krupa, Y.-J. Lee, P.D. Luckey, B. Maier, A.C. Marini, C. McGinn, C. Mironov, S. Narayanan, X. Niu, C. Paus, D. Rankin, C. Roland, G. Roland, Z. Shi, G.S.F. Stephans, K. Sumorok, K. Tatar, D. Velicanu, J. Wang, T.W. Wang, Z. Wang, B. Wyslouch

University of Minnesota, Minneapolis, USA

R.M. Chatterjee, A. Evans, S. Guts[†], P. Hansen, J. Hiltbrand, Sh. Jain, M. Krohn, Y. Kubota, Z. Lesko, J. Mans, M. Revering, R. Rusack, R. Saradhy, N. Schroeder, N. Strobbe, M.A. Wadud

University of Mississippi, Oxford, USA

J.G. Acosta, S. Oliveros

University of Nebraska-Lincoln, Lincoln, USA

K. Bloom, S. Chauhan, D.R. Claes, C. Fangmeier, L. Finco, F. Golf, J.R. González Fernández, I. Kravchenko, J.E. Siado, G.R. Snow[†], B. Stieger, W. Tabb, F. Yan

State University of New York at Buffalo, Buffalo, USA

G. Agarwal, H. Bandyopadhyay, C. Harrington, L. Hay, I. Iashvili, A. Kharchilava, C. McLean, D. Nguyen, J. Pekkanen, S. Rappoccio, B. Roozbahani

Northeastern University, Boston, USA

G. Alverson, E. Barberis, C. Freer, Y. Haddad, A. Hortiangtham, J. Li, G. Madigan, B. Marzocchi, D.M. Morse, V. Nguyen, T. Orimoto, A. Parker, L. Skinnari, A. Tishelman-Charny, T. Wamorkar, B. Wang, A. Wisecarver, D. Wood

Northwestern University, Evanston, USA

S. Bhattacharya, J. Bueghly, Z. Chen, A. Gilbert, T. Gunter, K.A. Hahn, N. Odell, M.H. Schmitt, K. Sung, M. Velasco

University of Notre Dame, Notre Dame, USA

R. Bucci, N. Dev, R. Goldouzian, M. Hildreth, K. Hurtado Anampa, C. Jessop, D.J. Karmgard, K. Lannon, N. Loukas, N. Marinelli, I. Mcalister, F. Meng, K. Mohrman, Y. Musienko⁴⁴, R. Ruchti, P. Siddireddy, S. Taroni, M. Wayne, A. Wightman, M. Wolf, L. Zygala

The Ohio State University, Columbus, USA

J. Alimena, B. Bylsma, B. Cardwell, L.S. Durkin, B. Francis, C. Hill, A. Lefeld, B.L. Winer, B.R. Yates

Princeton University, Princeton, USA

P. Das, G. Dezoort, P. Elmer, B. Greenberg, N. Haubrich, S. Higginbotham, A. Kalogeropoulos, G. Kopp, S. Kwan, D. Lange, M.T. Lucchini, J. Luo, D. Marlow, K. Mei, I. Ojalvo, J. Olsen, C. Palmer, P. Piroué, D. Stickland, C. Tully

University of Puerto Rico, Mayaguez, USA

S. Malik, S. Norberg

Purdue University, West Lafayette, USA

V.E. Barnes, R. Chawla, S. Das, L. Gutay, M. Jones, A.W. Jung, B. Mahakud, G. Negro, N. Neumeister, C.C. Peng, S. Piperov, H. Qiu, J.F. Schulte, M. Stojanovic¹⁵, N. Trevisani, F. Wang, R. Xiao, W. Xie

Purdue University Northwest, Hammond, USA

T. Cheng, J. Dolen, N. Parashar

Rice University, Houston, USA

A. Baty, S. Dildick, K.M. Ecklund, S. Freed, F.J.M. Geurts, M. Kilpatrick, A. Kumar, W. Li, B.P. Padley, R. Redjimi, J. Roberts[†], J. Rorie, W. Shi, A.G. Stahl Leiton

University of Rochester, Rochester, USA

A. Bodek, P. de Barbaro, R. Demina, J.L. Dulemba, C. Fallon, T. Ferbel, M. Galanti, A. Garcia-Bellido, O. Hindrichs, A. Khukhunaishvili, E. Ranken, R. Taus

Rutgers, The State University of New Jersey, Piscataway, USA

B. Chiarito, J.P. Chou, A. Gandrakota, Y. Gershtein, E. Halkiadakis, A. Hart, M. Heindl, E. Hughes, S. Kaplan, O. Karacheban²², I. Laflotte, A. Lath, R. Montalvo, K. Nash, M. Osherson, S. Salur, S. Schnetzer, S. Somalwar, R. Stone, S.A. Thayil, S. Thomas, H. Wang

University of Tennessee, Knoxville, USA

H. Acharya, A.G. Delannoy, S. Spanier

Texas A&M University, College Station, USA

O. Bouhali⁸⁸, M. Dalchenko, A. Delgado, R. Eusebi, J. Gilmore, T. Huang, T. Kamon⁸⁹, H. Kim, S. Luo, S. Malhotra, R. Mueller, D. Overton, L. Perniè, D. Rathjens, A. Safonov, J. Sturdy

Texas Tech University, Lubbock, USA

N. Akchurin, J. Damgov, V. Hegde, S. Kunori, K. Lamichhane, S.W. Lee, T. Mengke, S. Muthumuni, T. Peltola, S. Undleeb, I. Volobouev, Z. Wang, A. Whitbeck

Vanderbilt University, Nashville, USA

E. Appelt, S. Greene, A. Gurrola, R. Janjam, W. Johns, C. Maguire, A. Melo, H. Ni, K. Padeken, F. Romeo, P. Sheldon, S. Tuo, J. Velkovska, M. Verweij

University of Virginia, Charlottesville, USA

M.W. Arenton, B. Cox, G. Cummings, J. Hakala, R. Hirosky, M. Joyce, A. Ledovskoy, A. Li, C. Neu, B. Tannenwald, Y. Wang, E. Wolfe, F. Xia

Wayne State University, Detroit, USA

P.E. Karchin, N. Poudyal, P. Thapa

University of Wisconsin - Madison, Madison, WI, USA

K. Black, T. Bose, J. Buchanan, C. Caillol, S. Dasu, I. De Bruyn, P. Everaerts, C. Galloni, H. He, M. Herndon, A. Hervé, U. Hussain, A. Lanaro, A. Loeliger, R. Loveless, J. Madhusudanan Sreekala, A. Mallampalli, D. Pinna, T. Ruggles, A. Savin, V. Shang, V. Sharma, W.H. Smith, D. Teague, S. Trembath-reichert, W. Vetens

†: Deceased

- 1: Also at Vienna University of Technology, Vienna, Austria
- 2: Also at Department of Basic and Applied Sciences, Faculty of Engineering, Arab Academy for Science, Technology and Maritime Transport, Alexandria, Egypt
- 3: Also at Université Libre de Bruxelles, Bruxelles, Belgium
- 4: Also at IRFU, CEA, Université Paris-Saclay, Gif-sur-Yvette, France
- 5: Also at Universidade Estadual de Campinas, Campinas, Brazil
- 6: Also at Federal University of Rio Grande do Sul, Porto Alegre, Brazil
- 7: Also at UFMS, Nova Andradina, Brazil
- 8: Also at Universidade Federal de Pelotas, Pelotas, Brazil
- 9: Also at University of Chinese Academy of Sciences, Beijing, China
- 10: Also at Institute for Theoretical and Experimental Physics named by A.I. Alikhanov of NRC 'Kurchatov Institute', Moscow, Russia
- 11: Also at Joint Institute for Nuclear Research, Dubna, Russia
- 12: Now at British University in Egypt, Cairo, Egypt
- 13: Now at Cairo University, Cairo, Egypt
- 14: Also at Zewail City of Science and Technology, Zewail, Egypt
- 15: Also at Purdue University, West Lafayette, USA
- 16: Also at Université de Haute Alsace, Mulhouse, France
- 17: Also at Erzincan Binali Yildirim University, Erzincan, Turkey
- 18: Also at CERN, European Organization for Nuclear Research, Geneva, Switzerland
- 19: Also at RWTH Aachen University, III. Physikalisches Institut A, Aachen, Germany
- 20: Also at University of Hamburg, Hamburg, Germany
- 21: Also at Department of Physics, Isfahan University of Technology, Isfahan, Iran, Isfahan, Iran
- 22: Also at Brandenburg University of Technology, Cottbus, Germany
- 23: Also at Skobeltsyn Institute of Nuclear Physics, Lomonosov Moscow State University, Moscow, Russia
- 24: Also at Institute of Physics, University of Debrecen, Debrecen, Hungary, Debrecen, Hungary
- 25: Also at Physics Department, Faculty of Science, Assiut University, Assiut, Egypt
- 26: Also at MTA-ELTE Lendület CMS Particle and Nuclear Physics Group, Eötvös Loránd University, Budapest, Hungary, Budapest, Hungary
- 27: Also at Institute of Nuclear Research ATOMKI, Debrecen, Hungary
- 28: Also at IIT Bhubaneswar, Bhubaneswar, India, Bhubaneswar, India
- 29: Also at Institute of Physics, Bhubaneswar, India
- 30: Also at G.H.G. Khalsa College, Punjab, India
- 31: Also at Shoolini University, Solan, India
- 32: Also at University of Hyderabad, Hyderabad, India
- 33: Also at University of Visva-Bharati, Santiniketan, India
- 34: Also at Indian Institute of Technology (IIT), Mumbai, India
- 35: Also at Deutsches Elektronen-Synchrotron, Hamburg, Germany
- 36: Also at Department of Physics, University of Science and Technology of Mazandaran, Behshahr, Iran

-
- 37: Now at INFN Sezione di Bari ^a, Università di Bari ^b, Politecnico di Bari ^c, Bari, Italy
- 38: Also at Italian National Agency for New Technologies, Energy and Sustainable Economic Development, Bologna, Italy
- 39: Also at Centro Siciliano di Fisica Nucleare e di Struttura Della Materia, Catania, Italy
- 40: Also at Università di Napoli 'Federico II', NAPOLI, Italy
- 41: Also at Riga Technical University, Riga, Latvia, Riga, Latvia
- 42: Also at Consejo Nacional de Ciencia y Tecnología, Mexico City, Mexico
- 43: Also at Warsaw University of Technology, Institute of Electronic Systems, Warsaw, Poland
- 44: Also at Institute for Nuclear Research, Moscow, Russia
- 45: Now at National Research Nuclear University 'Moscow Engineering Physics Institute' (MEPhI), Moscow, Russia
- 46: Also at St. Petersburg State Polytechnical University, St. Petersburg, Russia
- 47: Also at University of Florida, Gainesville, USA
- 48: Also at Imperial College, London, United Kingdom
- 49: Also at P.N. Lebedev Physical Institute, Moscow, Russia
- 50: Also at Moscow Institute of Physics and Technology, Moscow, Russia, Moscow, Russia
- 51: Also at California Institute of Technology, Pasadena, USA
- 52: Also at Budker Institute of Nuclear Physics, Novosibirsk, Russia
- 53: Also at Faculty of Physics, University of Belgrade, Belgrade, Serbia
- 54: Also at Trincomalee Campus, Eastern University, Sri Lanka, Nilaveli, Sri Lanka
- 55: Also at INFN Sezione di Pavia ^a, Università di Pavia ^b, Pavia, Italy, Pavia, Italy
- 56: Also at National and Kapodistrian University of Athens, Athens, Greece
- 57: Also at Universität Zürich, Zurich, Switzerland
- 58: Also at Stefan Meyer Institute for Subatomic Physics, Vienna, Austria, Vienna, Austria
- 59: Also at Laboratoire d'Annecy-le-Vieux de Physique des Particules, IN2P3-CNRS, Annecy-le-Vieux, France
- 60: Also at Şırnak University, Şırnak, Turkey
- 61: Also at Department of Physics, Tsinghua University, Beijing, China, Beijing, China
- 62: Also at Near East University, Research Center of Experimental Health Science, Nicosia, Turkey
- 63: Also at Beykent University, Istanbul, Turkey, Istanbul, Turkey
- 64: Also at Istanbul Aydın University, Application and Research Center for Advanced Studies (App. & Res. Cent. for Advanced Studies), Istanbul, Turkey
- 65: Also at Mersin University, Mersin, Turkey
- 66: Also at Piri Reis University, Istanbul, Turkey
- 67: Also at Adiyaman University, Adiyaman, Turkey
- 68: Also at Ozyegin University, Istanbul, Turkey
- 69: Also at Izmir Institute of Technology, Izmir, Turkey
- 70: Also at Necmettin Erbakan University, Konya, Turkey
- 71: Also at Bozok Universiteleri Rektörlüğü, Yozgat, Turkey
- 72: Also at Marmara University, Istanbul, Turkey
- 73: Also at Milli Savunma University, Istanbul, Turkey
- 74: Also at Kafkas University, Kars, Turkey
- 75: Also at Istanbul Bilgi University, Istanbul, Turkey
- 76: Also at Hacettepe University, Ankara, Turkey
- 77: Also at School of Physics and Astronomy, University of Southampton, Southampton, United Kingdom
- 78: Also at IPPP Durham University, Durham, United Kingdom
- 79: Also at Monash University, Faculty of Science, Clayton, Australia

- 80: Also at Bethel University, St. Paul, Minneapolis, USA, St. Paul, USA
81: Also at Karamanoğlu Mehmetbey University, Karaman, Turkey
82: Also at Ain Shams University, Cairo, Egypt
83: Also at Bingol University, Bingol, Turkey
84: Also at Georgian Technical University, Tbilisi, Georgia
85: Also at Sinop University, Sinop, Turkey
86: Also at Mimar Sinan University, Istanbul, Istanbul, Turkey
87: Also at Nanjing Normal University Department of Physics, Nanjing, China
88: Also at Texas A&M University at Qatar, Doha, Qatar
89: Also at Kyungpook National University, Daegu, Korea, Daegu, Korea